Copy No. 7

DEFENCE R&D DÉFENSE

INTERPOLATION BEAMFORMING FOR A BENT ARRAY

D.N. Swingler

SAINT MARY'S UNIVERSITY

DEFENCE RESEARCH ESTABLISHMENT ATLANTIC

Contractor Report

DREA CR 1999-072

SEPTEMBER 1999

National Defence Défense nationale

Canada

National Defence
Research and Development Branch

Défense nationale
Bureau de recherche et développement

DREA CR 1999/072

Interpolation Beamforming For a Bent array

D.N. Swingler

Saint Mary's University
Halifax, NS, Canada
B3H 3C3

Scientific Authority Brian Maranda
B. Maranda

W7707-8-5996
Contract Number

September 1999

CONTRACTOR REPORT

Prepared for

Defence Research Establishment Atlantic

Centre de Recherches pour la Défense Atlantique

Canada

ABSTRACT

The performance of a computationally efficient interpolation beamformer is investigated. For each snapshot, each beam's output is formed from the weighted sum of relatively few Fourier coefficients taken from the Fast-Fourier transform of the narrowband sensor data. The weights perform an interpolation action on the Fourier coefficients and can be chosen to offer both array shading and bend compensation. A simple rule-of-thumb is given for the minimum number of weights necessary for Kaiser-Bessel shading of a uniform line-array bent into an arc of a circle of known radius.

It is demonstrated, via numerical simulations, that such an interpolation beamformer has a beampattern which is within about 0.1 dB of that of the benchmark delay-and-sum beamformer over the important mainlobe and near-in sidelobes.

It is also shown that the interpolation beamformer can be used in a wideband active sonar scenario involving linear FM chirps and correlation detection.

RÉSUMÉ

Le document examine la performance d'un conformateur de faisceau à interpolation efficace sur le plan du calcul. Pour chaque valeur instantanée, la sortie des différents faisceaux est conformée à partir de la somme pondérée des coefficients de Fourier relativement peu nombreux, qui résultent de la transformation de Fourier rapide appliquée aux données de capteur à bande étroite. Les pondérations ont un effet d'interpolation sur les coefficients de Fourier et peuvent être choisis de façon à permettre la compensation d'ombrage et de courbure de l'antenne réseau. Une règle empirique simple est donnée relativement au nombre minimal de pondérations que nécessite l'effet d'ombrage de Kaiser-Bessel dans le cas d'un réseau linéaire uniforme recourbé en arc de cercle de rayon connu.

Des simulations numériques démontrent que ce conformateur de faisceau à interpolation produit un diagramme de faisceau dont l'écart par rapport à celui du conformateur de faisceau à retard et somme de référence n'excède pas environ 0,1 dB dans l'important lobe principal et dans les lobes latéraux rapprochés.

Il est également démontré que le conformateur de faisceau à interpolation peut s'utiliser dans un système sonar actif à large bande permettant la modulation de fréquence linéaire et la détection de corrélation.

Interpolation Beamforming for a Bent Array

LIST OF CONTENTS

1. Introduction 1-1

2. Interpolation beamforming for a uniform line-array 2-1
   2.1 Introduction 2-1
   2.2 Simulation experiments 2-4
      2.2.1 Case where N=M=128. 2-4
      2.2.2 Case where N=65, M=128 2-7
      2.2.3 Case where M=N=64. 2-8
      2.2.4 Summary 2-8
   2.3 Effect of reallocating the shading function 2-9

3. Interpolation beamforming with a bent array 3-1
   3.1 Introduction 3-1
   3.2 An approximate expression for M2 3-3
   3.3 SNR calculations 3-4
   3.4 Some simulation experiments 3-5
      3.4.1 Experiments near broadside 3-5
      3.4.2 Experiments near endfire 3-6
      3.4.3 Experiments with N/M ≈ 0.5 3-8
      3.4.4 Some plots of the bend correction filter, $C(p,\theta_0)$ 3-9
   3.5 Simulation experiments over 0-360^0 3-9
   3.6 Summary 3-12

4. Interpolation beamforming for an active sonar. 4.1
4.1 Introduction 4-1
4.2 Simulation results 4-2
4.3 Summary 4-3

5. Conclusion 5.1

6. References 6.1

1. Introduction

This report represents an investigation into efficient planewave beamforming using a bent line-array. The unbent array is a uniform line-array and, for simplicity, the curvature of the bent array takes the form of an arc of a circle of known radius.

Conventional, narrowband, delay-and-sum beamforming is easily applied to such a bent array but if there are N sensors, and N beams are to be computed, then the total computational load is of the order of N^2 operations per snapshot. A more efficient approach was suggested recently by Dalrymple [1-1] , building on an concept of DeMuth [2-1], wherein the narrowband (NB) sensor data is Fast-Fourier transformed and relatively few, M, say, of these Fourier coefficients are then used to produce each output beam sample. Hence, very roughly, the computational load is now on the order of $MN+M\log_2(N)$. Operating on M adjacent Fourier coefficients to provide an estimate of the output of a beam whose direction may not coincide exactly with any of the underlying M beam directions is essentially an interpolation problem and for this reason the beamformer under study is known as an "interpolation beamformer".

The primary goal of this report is to provide a more thorough treatment of appropriate choice of M, the number of interpolator weights, than that given by Dalrymple. The number should be small for efficiency reasons yet must be large enough to provide adequate beamforming performance, especially in the presence of significant array curvature. Among the parameters that influence M are the number of sensors, the size of the FFT, the extent of the curvature and the choice of array shading.

We shall demonstrate that it is useful to decompose M into the sum of two values, one dealing with the creation of the appropriate shading effect with an unbent array, the other dealing with the array curvature. Where the curvature is significant, the latter is the

dominant effect. For Kaiser-Bessel shading we give a simple rule-of-thumb for the choice of M in any given scenario.

Finally, we demonstrate that this approach can also be used in a wideband, active sonar scenario.

2. Interpolation beamforming for a uniform line-array

2.1 Introduction

Consider a uniform line-array with N sensors operating at a temporal frequency, f Hz. If the complex-valued Fourier coefficient from the nth sensor is written as $X(n)$ then the beam output at angle θ with respect to broadside may be written as the sum

$$B(\theta) = \sum_{n=0}^{N-1} X(n)\, W(n) \exp(-j\, k\, n\, d \sin(\theta)) \qquad (2.1)$$

where d is the element spacing, $k = 2\pi f / c$ and c is the acoustic propagation speed. $W(n)$ is the shading function applied to reduce the inevitable sidelobes due to source(s) at other angle(s).

Efficient computation of (2.1) over a set of beam angles is possible via the FFT algorithm if the argument $kd \sin(\theta) = 2\pi m / M$ where m, M are integers with $M \geq N$. We shall assume a radix-2 FFT algorithm with M chosen as that radix-2 value not less than N and closest to it. Zero-padding of the N terms of $X(n)$, $W(n)$ in (2.1) prior to FFT'ing is necessary if $M>N$. If the FFT process can be used directly, we rewrite (2.1) as

$$B(\theta) = \sum_{n=0}^{M-1} X(n)\, W(n) \exp(-j\, 2\pi m n / M) \qquad (2.2)$$

Equation (2.2) implies that the beam angle(s) of interest correspond exactly to FFT cells[1]. The more usual situation occurs, however, where all the beam angles do not meet this criterion. To deal with the latter circumstance, following DeMuth [2-1], we recognize

[1] We shall use the phrase "FFT cell" in spatial frequency processing in an analogous fashion to the corresponding phrase "FFT bin" in temporal frequency processing.

that for a particular beam angle, θ, the spatial frequency $kd\sin(\theta)$ must be "close" to an FFT cell so that we can combine (2.1) and (2.2) as

$$B(\theta) = \sum_{n=0}^{M-1} X(n)\, W(n) \exp(-j2\pi ns / M) \exp(-j2\pi nm / M) \qquad (2.3)$$

In (2.3), $2\pi(m+s)/M = kd\sin(\theta)$ and we let m be the integer such that $2\pi m/M$ is closest to $kd\sin(\theta)$. The residual is $2\pi s/M$ where $|s| \le 1/2$. Note that m and s are both functions of θ.

A further perusal of (2.3) reveals that we are performing an DFT (in practice an FFT) on a product of terms and we know that this can be expressed as a circular convolution in the spatial domain

$$B(\theta) = \frac{1}{M} \sum_{p=0}^{M-1} Y(m-p)\, w_s(p)$$

where $Y(p)$ and $w_s(p)$ represent the M-point DFT (FFT in practice) of $X(n)$ and $W(n)\exp(-j2\pi ns/M)$ (zero-padded, if necessary), respectively. Note that functions $Y(p)$ and $w_s(p)$ are periodic in M. Note also that there is no frequency dependence associated with the shading function, but there is an explicit dependence on the fractional steering quantity, s.

For our purposes it is convenient to approximate the above expression by

$$B(\theta) = \frac{1}{M} \sum_{p=-(M1-1)/2}^{(M1-1)/2} Y(m-p)\, w_s(p) \qquad (2.4)$$

Equation (2.4) represents interpolation. In essence, the $w_m(p)$ function predominantly weights the $Y(p)$ values in the region centered on FFT cell number m to produce the desired result which combines both steering and shading It is of quintessential concern to us to understand just how many terms, $M1$, are actually needed in the summation of (2.4) to produce acceptable results. If only a "few" terms are necessary ($M1 \ll N$, say) then (2.4) offers an efficient, FFT-based, beamforming method wherein the FFT operation is used to compute $Y(p)$ and (2.4) is used, with a limited number of pre-computed weights, $w_m()$, to give the beam output. If "many" terms ($M1 \sim N$) are needed from $w_m()$ then the efficiency is lost and we may as well perform the brute-force DFT summation explicit in (2.1) for each beam.

The first task, then, is to ascertain the inter-relationships as they apply to beamforming performance, among the following items:

(i) Choice of shading function. In this report we shall concentrate exclusively on the Kaiser-Bessel window, though the MATLAB simulations written for the this project also include a Hamming window option.

(ii) Number of retained terms, $M1$, in the interpolation of (2.4).

(iii) Ratio N/M which, due to the radix-2 assumption, must lie between 0.5 and 1.

(iv) Temporal frequency ratio, f/f_c where f_c is the frequency for which the inter-element spacing, d, is one-half wavelength. We assume $f/f_c \leq 1$.

(v) Whether the shading function is applied to the fractional steering term, $\exp(-jknm\sin(\theta))$ as implied above, or whether it is applied to the array data $X(n)$ prior to the FFT being taken. In the latter case the interpolation function is that of a uniformly-shaded array, i.e. approximately a sinc function.

The performance measures will be the maximum sidelobe height in the response to a single plane wave source, the mainlobe gain and the mainlobe width. Each is expected to be negatively affected by a reduction in the number of interpolating coefficients retained in $w_s 0$.

2.2 Simulation experiments

2.2.1 Case where N=M=128.

We start by examining the output of a uniform line array with $N = 128$ sensors using an FFT length M=128. If the "cut" frequency is f_c, defined as that frequency for which the element spacing d is equal to one-half wavelength, then we may write $kd\sin(\theta) = \pi(f / f_c)\sin(\theta)$ and the simulation can be handled entirely in terms of the frequency ratio $f_r = f / f_c$ without recourse to explicit values of d, c, f.

Further, recall from the above that $kd\sin(\theta) = 2\pi(m+s)/M$ hence we have $\pi f_r \sin(\theta) = 2\pi(m+s)/M$. It will be useful to write

$$\pi f_r \sin(\theta) = 2\pi\Psi / M \qquad (2.5)$$

where $\Psi = m+s$ is interpreted as the location corresponding to the bearing, θ, measured in FFT cells pertaining to our length-M FFT. It may be non-integer. We also note that the quantity $2\pi / M$ corresponds to the beamwidth (mainlobe peak to first zero) of a uniformly shaded array of length M.

The quantity Ψ will be used in this report to denote the location of the single source in our experiment. Numerically, it is the distance of the source from broadside, measured in beamwidths. It subsumes d, f, f_c and θ. The symbol Ψ_0 will be used to denote the beam, or steering, direction. As Ψ_0 must be decomposed into $m + s$ and the

interpolation function $w_s(p)$ is dependent on s, we must repeat the experiment over a representative set of values for $|s| \leq \frac{1}{2}$.

Having chosen N=128 sensors, we arbitrarily let the steering direction Ψ_0 vary from 20 to 20.5 in steps of 0.1; this is equivalent to fixing $m = 20$ with s varying from 0 to 0.5 in steps of 0.1 (See footnote[2]). For each value of steering direction, we let the source location, Ψ, vary from 10 to 30. The results are shown in Fig. 2.1 for the case where we utilize the dominant $M1 = 63$ terms of the $w_s(p)$ function in the convolution of (2.4).

In Fig. 2.1 the results are arranged from Ψ_0=20 in the upper left to Ψ_0=20.5 in the lower right. We note that all the results are similar, indicating negligible sensitivity to the fractional steering parameter, s. The curves are normalized to a peak of 0dB for the full 128-point convolution for each s. There is negligible mainlobe loss using $M1$=63 points. The Kaiser-Bessel window function was chosen with a parameter of α=1.3 which yields a maximum sidelobe level of -30dB with respect to the mainlobe peak[3] . Careful inspection of the data in Fig. 2.1 reveals that the peak sidelobes are indeed at -30dB.

In order to demonstrate the steering action more closely, the simulation is re-run over a smaller range of source locations as shown in Fig. 2.2. We now see clearly that the location of each mainlobe peak coincides with the corresponding steering angle, Ψ_0, as expected.

Fig. 2.2 also permits a measurement of the mainlobe width. It will be arbitrarily, but conveniently, characterized by the half the separation between the -20dB points on the mainlobe, again measured in FFT cells. From Fig. 2.2 we see this is about $\Delta\Psi = 1.4$ or about 40% greater than the beamwidth of an unshaded array (with N=M) measured from peak to first zero ($\Delta\Psi$=1).

---

[2] Note that only positive values of s will be examined here. As might be expected from symmetry arguments, the results using the corresponding negative values are identical and will be eschewed for space reasons.

We are interested in the performance associated with smaller values of $M1$ and Fig. 2.3 displays the corresponding results to Fig. 2.1 but for $M1$=15. The results are little different from those in Fig. 2.1 implying little performance penalty for this value of $M1$. However the convolution computation effort in (2.4) is significantly reduced.

At this point it is convenient to investigate the $w_s(p)$ weights in more detail. As mentioned earlier these are taken from the length-M FFT of the length-N, phase-shifted, Kaiser-Bessel window function, $W(n)\exp(-j2\pi ns/M)$, zero-padded if necessary. In our case M=N=128 and no zero padding is involved.. Fig. 2.4(a), (b), (c) show the magnitudes of the weights truncated to $M1$=15 for s=0, s=0.25 and s=0.5, respectively. These are taken as representative and have been normalized such that $\sum_{n=0}^{M-1} W(n)=1$. As might be expected the values at the left and right extremities are close to zero which explains why the impact of truncation has heretofore been insignificant. Indeed if we argue that values less than 0.032 (i.e. -30dB with respect to peak value of unity) are negligible than we observe from Fig. 2.4 that truncation down as low as $M1$=5 seems reasonable.

Fig. 2.5 shows the beam outputs for the case where $M1$=5. We now see some noticeable differences in the sidelobe structures. Careful examination reveals the most significant effect is that the peak sidelobe level is (for s=0.5) now about -26.8dB, about 3.2dB above the nominal design level. However, there is little difference in the mainlobe gains or widths from the previous cases with larger values of $M1$.

Obviously if the -30dB sidelobe constraint is to be maintained, then it is necessary either to increase the value of $M1$, with a concomitant increase in computational burden, or to increase the Kaiser-Bessel parameter with a concomitant increase in mainlobe width.

For the sake of completeness, the peak sidelobe levels were recorded for the Kaiser-Bessel window ($\alpha = 13$) with M=N=128 for $M1$={5, 7, 9, 11, 13, 15} as {-26.8, -28.3, -28.7, -29.1, -29.4, -29.7}dB, respectively.

2.2.2 Case where N=65, M=128

We have adopted the notion that FFT length M is the nearest radix-2 value greater than the number of sensors, N. An extreme case occurs where M=128 and N=65. In this case we require zero-padding of length 63 prior to FFT'ing and the ratio N/M is close to 0.5. This has an impact on our processing as there is now considerable leakage of $Y(p)$ into adjacent FFT cells even if the source location Ψ is integer. This implies that it will be necessary to retain more interpolator weights to deal with these wider structures. Indeed it would seem reasonable to anticipate that if the minimum number of weights in the previous case (N/M=1) is $M1$=5, then in our new scenario the minimum number might be $M1$=5(M/N) or approximately, 10. As our simulations are written with $M1$ odd, we anticipate useful results for $M1$=11.

Fig. 2.6 shows the results for the case with N=65, M=128, $M1$=11. We see that the lobe structures are about twice as wide as the earlier scenarios but otherwise the results are very close to those of Fig. 2.5 where $M1$=5. If we reduce $M1$ to 5 in the current scenario, the peak sidelobes increase by a further 2.5dB to about -24.3dB (for s=0.5).

Rule-of-thumb:

As a result of running many simulations of the above type, it became obvious that there is a useful rule-of-thumb for calculating the minimum number of weights, $M1$, for "acceptable" processing. It is as given above;

$$M1 = M1^{\circ}\ (M / N) \qquad (2.6)$$

where $M1^{\circ}$ is the minimum acceptable number of weights for the case where M/N=1. In our case $M1^{\circ}$ is chosen as about 5.

2.2.3 Case where M=N=64.

We now briefly examine the impact of changing both the number of sensors and the size of the FFT. We choose M=N=64 with a view to exploring whether this has any impact on our above "rule-of-thumb".

Fig. 2.7 shows the situation where $M1$=$M1^0$ = 5 and where M=N=64. We see little difference with respect to Fig. 2.4 indicating that $M1^0$ = 5 remains a reasonable choice, even though the number of sensors has been halved, as M/N remains unity.

Fig. 2.8 show results for N=33, M=64. Following our rule of thumb we expect reasonable results for $M1$=11 and indeed the results in Fig. 2.8 are very similar to those in Fig. 2.6.

2.2.4 Summary

The results shown here, along with many others run during the course of the investigation, have suggested that the acceptable interpolation processing of N-sensor data, via an M-point FFT using a Kaiser-Bessel window, with nominally -30dB sidelobes, is available with $M1$ interpolation weights where

$$M1 = M1^0 \ (M / N) \qquad (2.6)$$

If $M1^0 \approx 5$ then there is a increase in the peak sidelobe level of about 3dB for the worst case, s = 0.5. This result is independent of (a) frequency; (b) absolute values of M and N; and (c) apart from the subtle impact of s, the steering direction.

In passing it might be remarked that foregoing comments remain generally valid even when a Hamming window is used in place of the Kaiser-Bessel.

2.3 Effect of reallocating the shading function

Equation (2.3) has been interpreted as the DFT of the product of the data, $X(n)$, and the shading/steering function, $W(n)\exp(-j2\pi ns/M)$. It is of interest to briefly examine the impact of regrouping these as $X(n)W(n)$ and $\exp(-j2\pi ns/M)$ so that the shading function is now associated with the data, and the fractional steering function effectively has uniform shading. While this may seem to be a benign operation in terms of linear system theory, it transpires that when truncation of the $w_s(p)$ interpolator (now, of course, samples from a sinc function) is taken into account, the results are inferior to those presented earlier.

As an example, we reprocess the case where M=N=128 and $M1$=5 with this reallocation of $W(n)$ to yield the results of Fig. 2.9(a). In comparison with Fig. 2.5 we note large sidelobe levels, especially those for Ψ_0=20.5 (i.e. s=0.5) which are at about -18dB. This is unacceptable.

If we increase the number of interpolator weights to $M1$=15 we have the results of Fig. 2.9(b). Here the peak sidelobes are reduced to -30dB but are somewhat disconcerting in appearance. It is worth noting that there are two predominant sidelobes whose locations correspond to the two points where the source mainlobe moves outside the interpolation interval. Hence the separation between them is approximately $M1$.

It would seem then that there is good reason for us to continue to allocate the shading function to the to the fractional steering term rather than to the data.

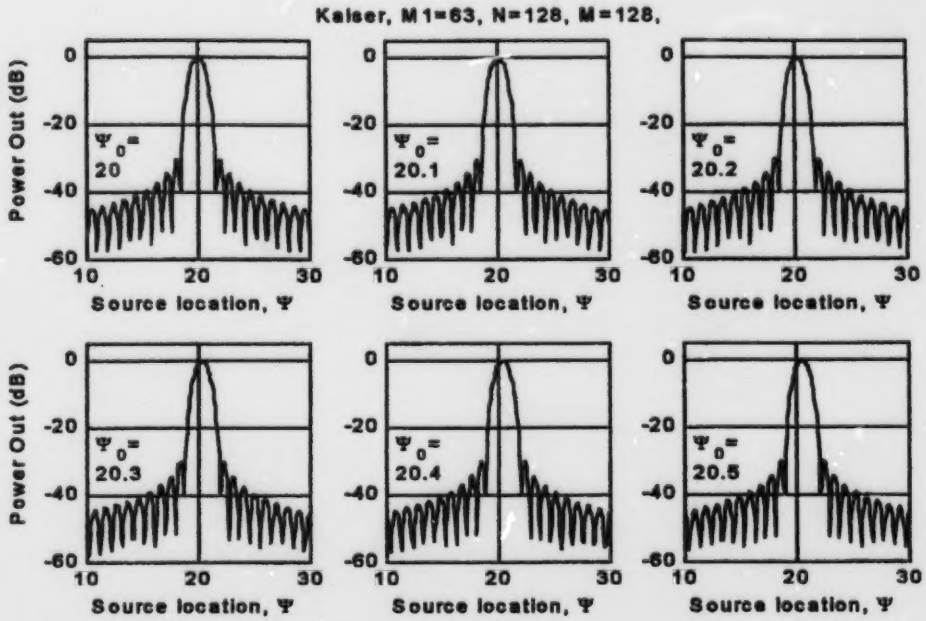

Fig. 2.1. Beam outputs for N=M=128, $M1$=63.

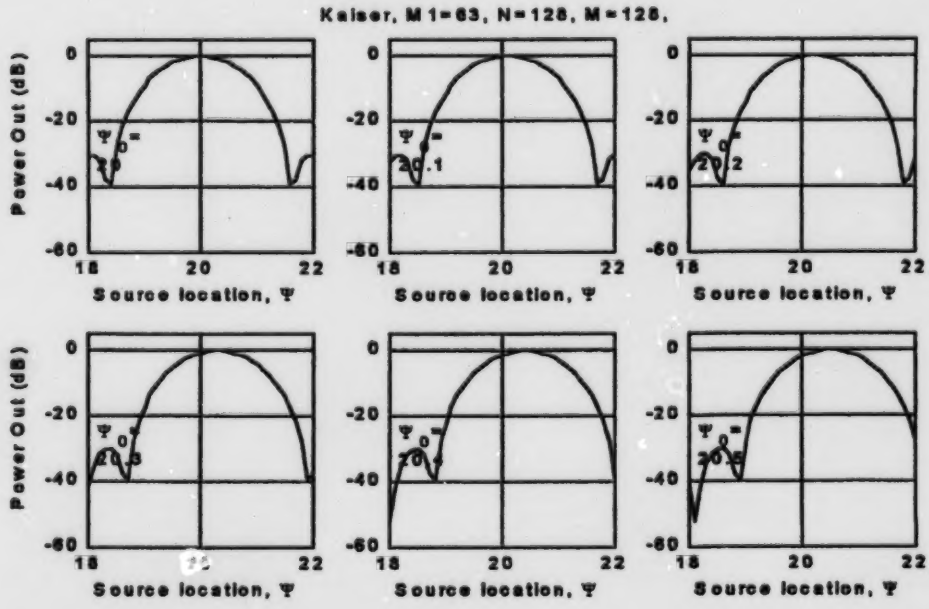

Fig. 2.2. As Fig.2.1 but showing mainlobe shift

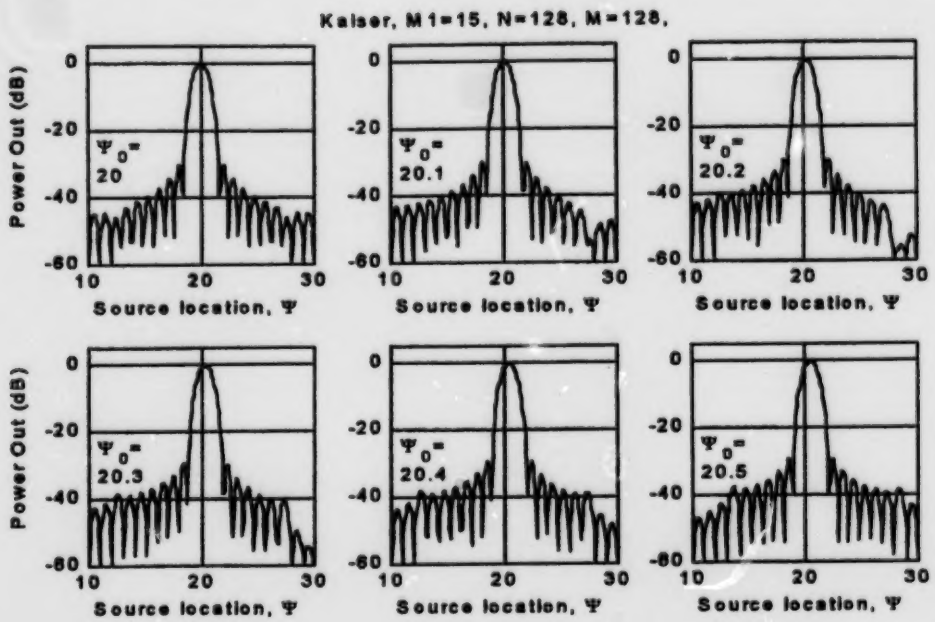

Fig. 2.3 Beam outputs for M=N=128, $M1$=15

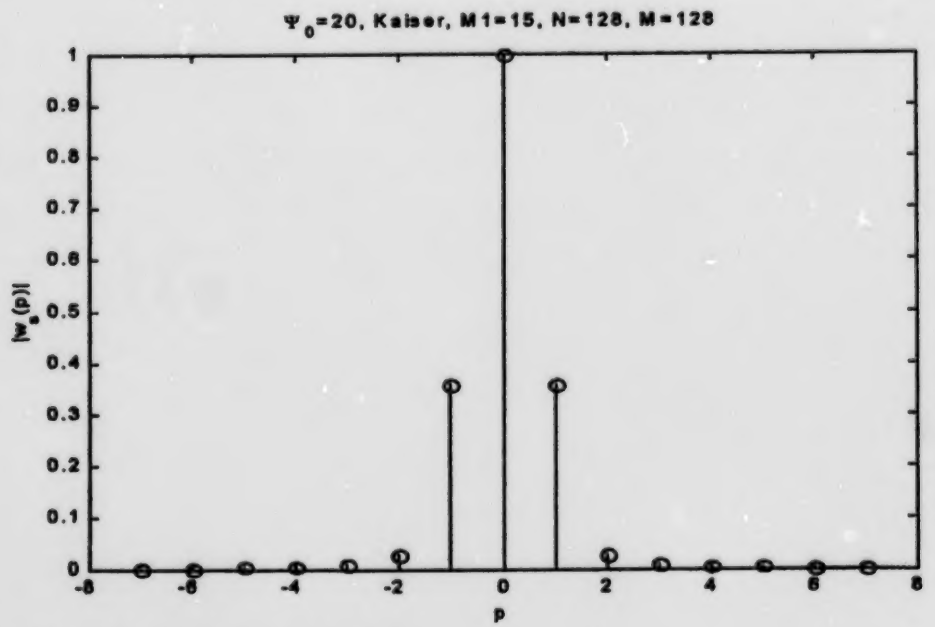

Fig. 2.4(a) Interpolation weights (s=0)

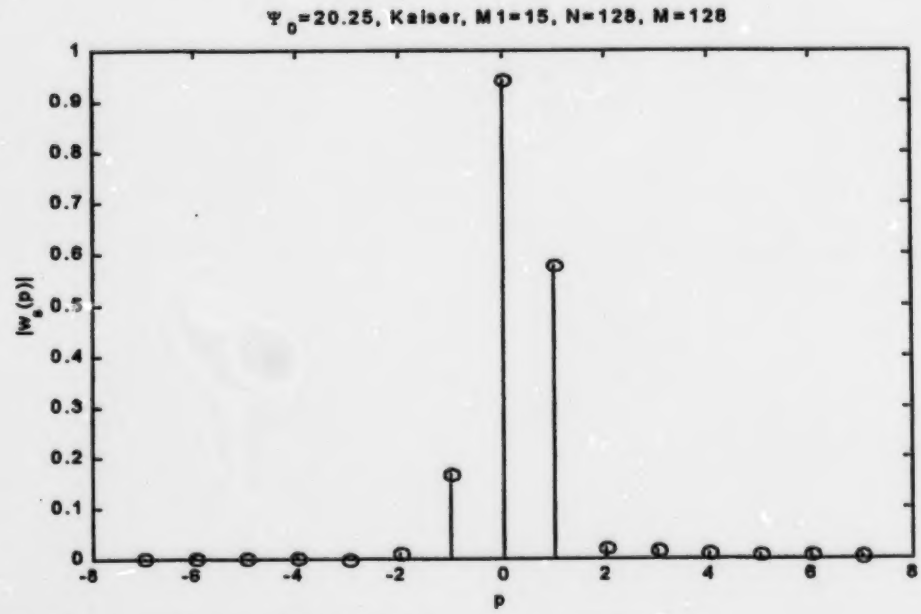

Fig. 2.4(b) Interpolation weights (s=0.25)

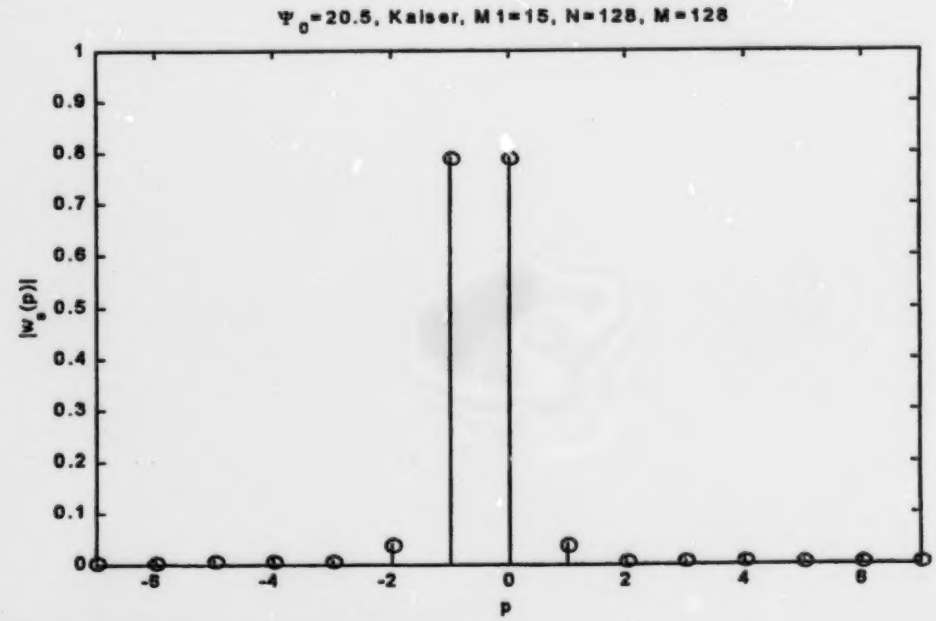

Fig. 2.4(c) Interpolation weights (s=0.5)

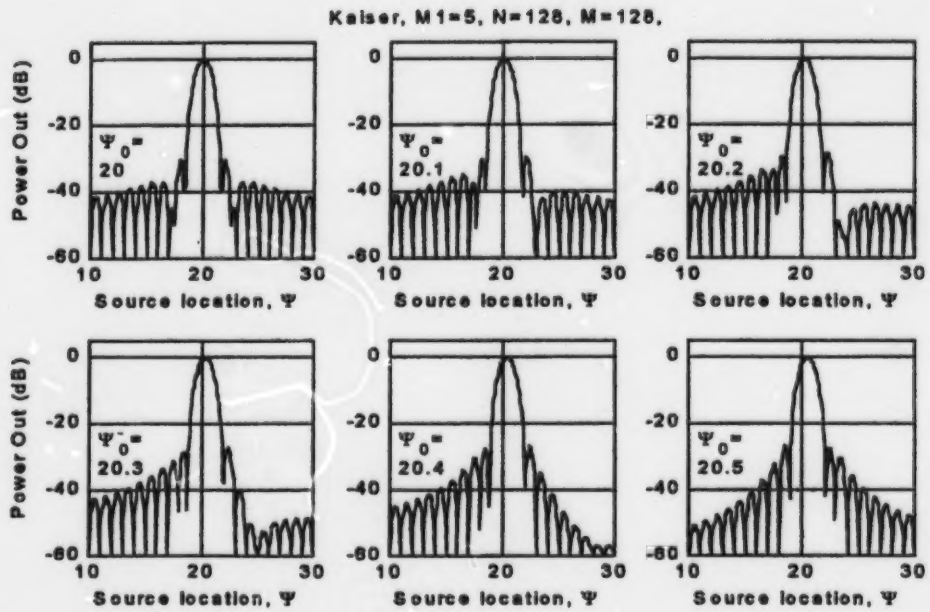

Fig. 2.5 Beam outputs for N=M=128, $M1$=5.

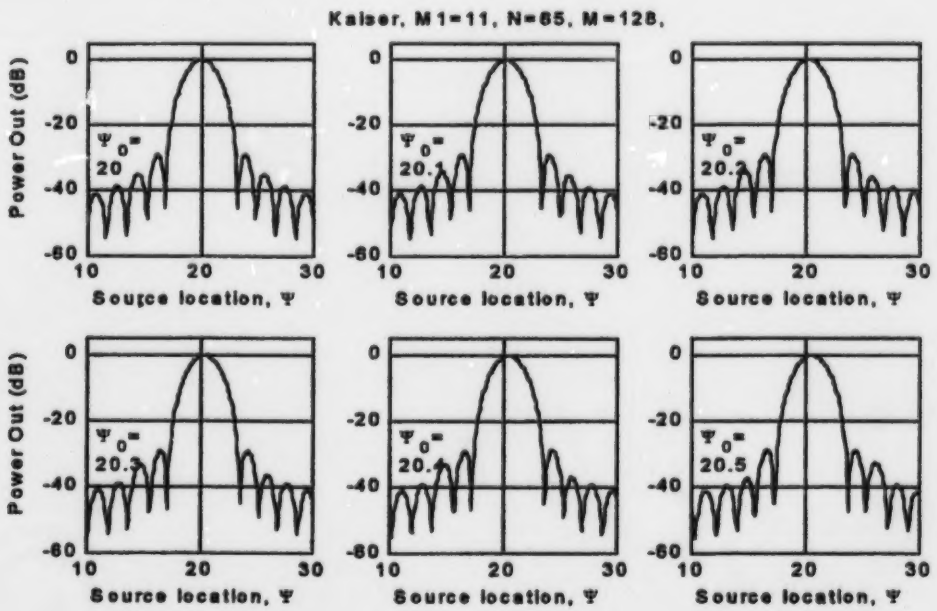

Fig. 2.6 Beam outputs for N=65, M=128, $M1$=11.

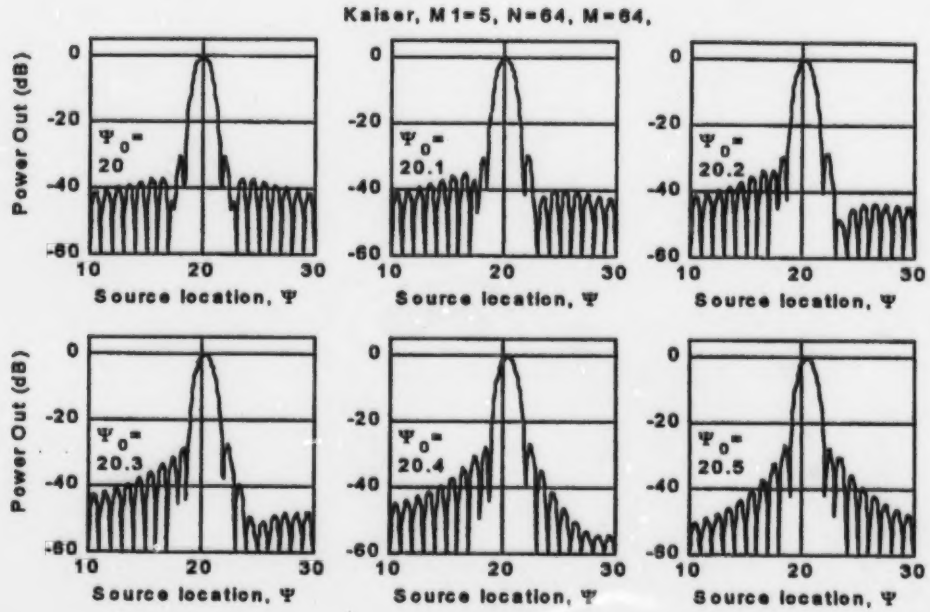

Fig. 2.7 Beam outputs for M=N=64, $M1$=5.

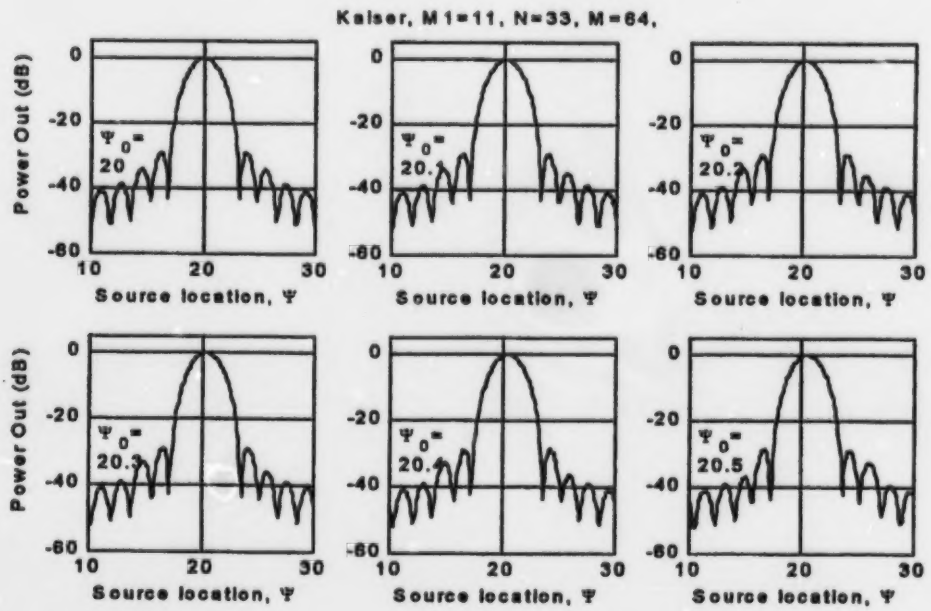

Fig. 2.8 Beam outputs for N=33, M=64, $M1$=11.

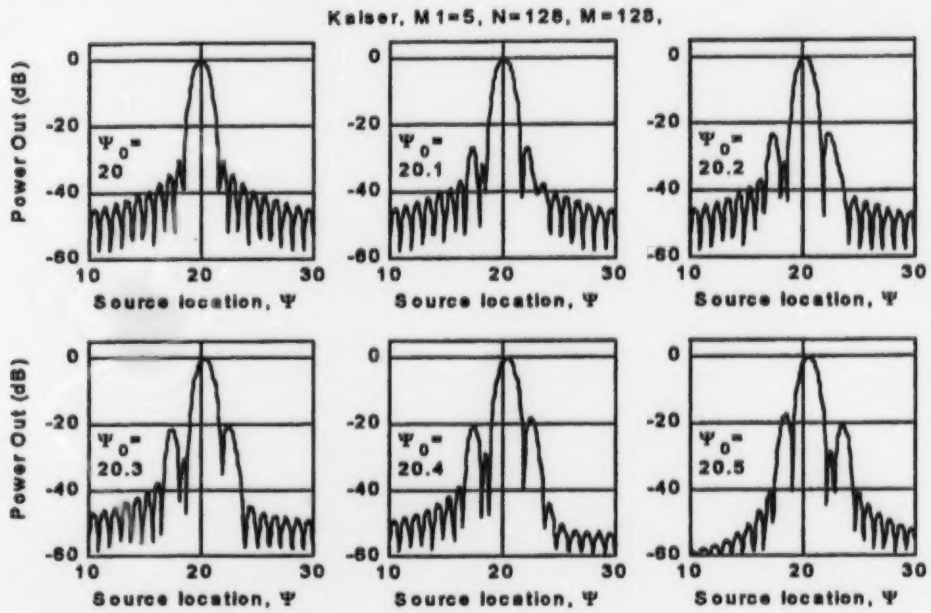

Fig. 2.9(a) Effect of associating the shading directly with the data. M=N=128, $M1$=5.

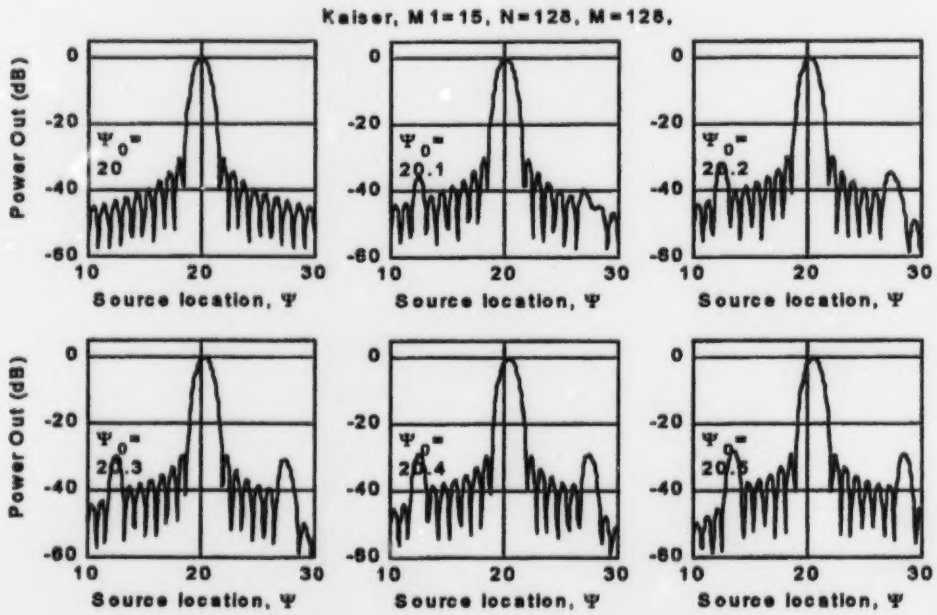

Fig. 2.9(b) As Fig. 2.9(a) but with $M1$=15.

3. Interpolation beamforming with a bent array

3.1 Introduction

We now move on to consider a bent line array of N elements. The situation is sketched in Fig. 3.1 where the bent array takes the form of an arc of a circle which has the unbent uniform line-array as a chord joining the endpoints. The maximum bow at the centre of the array is D and the n^{th} sensor has a y-coordinate given by

$$y_n = D\left(1-\left(\frac{2x_n}{(N-1)d}\right)^2\right) \tag{3.1}$$

This assumes that the bow is relatively small compared to the array length and that the x-coordinate is unaffected by the bend.

The output of a conventional narrowband, planewave, delay-and-sum beamformer (CBF) steered in direction, θ_0, may be written as

$$B(\theta_0) = \sum_{n=0}^{N-1} X(n)W(n)\exp(jky_n\cos(\theta_0))\exp(-jknd\sin(\theta_0)) \tag{3.2}$$

where $X(n)$ represents the NB output from the nth sensor of the bent array. The term involving y_n compensates for the bend.

While (3.2) may be implemented directly, we are interested in a possibly more efficient method based on the interpolation beamformer (IBF) of the previous section. Following the earlier discussion, an efficient implementation may take the form of a spatial convolution as indicated in (2.4). In order to compensate for the bend, (2.4) may be re-written as a convolution equivalent to (3.2):

$$B(\theta_0) = \frac{1}{M} \sum_{p=-(\tilde{M}-1)/2}^{(\tilde{M}-1)/2} Y(m-p)\tilde{w}_s(p) \tag{3.3}$$

where $\tilde{w}_s(p)$ is the DFT of $W(n)\exp(jky_n\cos(\theta_0))\exp(-2\pi ns/M)$ and $Y(p)$ represents the DFT of the sensor outputs, $X(n)$. Note that the number of retained terms in the convolution is explicitly set to $\tilde{M}$ ($\geq M1$ of previous section). The m and s values are the integer and fractional steering quantities discussed earlier.

Obviously, the $\tilde{w}_s(p)$ interpolator in (3.3) may itself be written as a convolution of the interpolator for the unbent array, $w_s(p)$, and the DFT of the bend-correction term, $\exp(jky_n\cos(\theta_0))$. If the latter is defined as $C(p,\theta_0)$, then we have

$$\tilde{w}_s(p) = \frac{1}{M}\sum_q w_s(p-q)C(q,\theta_0) \tag{3.4}$$

Again, for efficient implementation, it is important to minimise both the number of terms in the summation and the number of p values in the result of (3.4). We take the approach that the length of $w_s(.)$ may be truncated to the value of $M1$ according to the unbent scenarios of the last section (typically $M1 = 5M/N$, as in (2.6)). The truncation length, $M2$, for $C(.)$ is yet to be determined. In the case of an unbent array, $M2 = 1$. For given values of $M1$ and $M2$, the length of $\tilde{w}_s(p)$, and hence the number of retained terms in the primary convolution summation (3.3), is

$$\tilde{M} = M1 + M2 - 1 \tag{3.5}$$

As might be expected, we shall demonstrate that $M2$, and consequently $\tilde{M}$, increases as the amount of bow increases.

Finally it should be emphasized that bend correction is a function of the cosine of the steering direction, θ_0, and it is therefore necessary to explore the effects of bend correction over bearings in the full 0-360^0 range.

3.2 An approximate expression for *M2*

From the above, we have the bend correction term, $\exp(jky_n\cos(\theta_0))$. Working on the spatial equivalent, $\omega(x)$, of 'instantaneous frequency' we may define

$$\omega(x) = \frac{\partial}{\partial x}\left(ky\cos(\theta_0)\right) = \frac{\partial}{\partial x}\left(kD\left[1-\left(\frac{2x}{d(N-1)}\right)^2\right]\cos(\theta_0)\right)$$

$$= \frac{-8kDx\cos(\theta_0)}{d^2(N-1)^2} \text{ rad/m} \qquad (3.6)$$

which is zero at the centre of the array (x=0) and is maximal at the end points of the array ($|x| = (N\text{-}1)d/2$). Hence the spatial frequency extrema are

$$\omega_{max} = \frac{4kD|\cos(\theta_0)|}{d(N-1)} \text{ and } \omega_{min} = \frac{-4kD|\cos(\theta_0)|}{d(N-1)} \text{ rad/m}$$

If we are using M-point FFT's then the FFT cell width is $2\pi/(dM)$ rad/m implying that the bend correction term, $C(p,\theta_0)$, roughly spans $(\omega_{max}-\omega_{min})/(2\pi/(dM)) = 8DM|\cos(\theta)|/((N-1)\lambda)$ cells which, as $N>>1$, is approximately

$$\frac{8D|\cos(\theta_0)|}{\lambda}\frac{M}{N} \text{ cells} \qquad (3.7)$$

As the convolutions are performed in the context of such FFT cells, we might therefore conclude that

$$M2 \approx 8DM\,|\cos(\theta_0)|\,/(\lambda N). \tag{3.8}$$

Rule-of-thumb:

Equation (3.8) forms the basis of a working formula given by (a) replacing the cosine term by its maximum value of unity; (b) adding on an arbitrary constant of value seven to the $8D/\lambda$ term to account for the conservative nature of the approximation (3.8), especially at low values of D/λ. This yields the following rule-of-thumb[1]:

$$M2 = \left(8\frac{D}{\lambda} + 7\right)\frac{M}{N} \tag{3.9}$$

The utility of (3.9) will be demonstrated in the following simulations.

3.3 SNR calculations

At this point it is convenient to introduce an SNR measure. For a narrowband signal of magnitude |A|, measured at the sensors, in uncorrelated noise of variance σ^2, the output SNR of an N-element CBF steered in the direction of the signal is:

$$SNR(CBF) = \frac{|A|^2\left(\sum_{n=1}^{N} W(n)\right)^2}{\sigma^2 \sum_{n=1}^{N} W^2(n)}. \tag{3.10}$$

[1] It will be noticed that (3.9) does not have the desirable property that $M2 \to 1$ as $D/\lambda \to 0$. An alternative version with this property is given by multiplying the right-hand side of (3.9) by $(1-\exp(-20D/\lambda))$ then adding one. The modification is useful only for small D/λ and is eschewed here for simplicity.

For the corresponding IBF, the calculations are more appropriately performed in the spatial-frequency domain. If we assume an N-point FFT applied to the sensor data then,

$$SNR(IBF) = \frac{\left(\sum_{p=-(\tilde{M}-1)/2}^{(\tilde{M}-1)/2} \tilde{Y}_0(m-p)\tilde{w}_s(p) \right)^2}{N\sigma^2 \sum_{p=-(\tilde{M}-1)/2}^{(\tilde{M}-1)/2} \tilde{w}_s^{\,2}(p)} \qquad \text{---(3.11)}$$

where $\tilde{Y}_0(n)$ represents the DFT of the signal components (magnitude, |A|) measured across the sensors.

3.4 Some simulation experiments

3.4.1 Experiments near broadside.

We start by examining the beamformer response to a single source in the vicinity of broadside. Following Section 2, we adopt the approach that the response may be usefully examined on expressing the source location in FFT cell units, Ψ, (see equation 2.5). Fig. 3.2(a) shows the response, or beampattern, for steering directions, $\Psi_0 = 0$, 0.1, 0.2, 0.3, 0.4 and 0.5. In this particular case, the fractional steering parameter, s, is given by $s = \Psi_0$. As annotated on the figure we have M=N=128 and f_t=1. The array is perfectly linear, $D/\lambda = 0$, and so, again following Section 2, we set $M1$=5 and $M2$=1. With $M2 = 1$, there is no bend compensation.

Fig. 3.2(a) gives us the benchmark against which the effectiveness of our interpolation beamformer can be assessed. We recall that the peak sidelobe levels, nominally set to -30dB via the Kaiser shading, do increase with s to about -27dB.

In Fig. 3.2(b) we increase D/λ to 0.25 and set $M2$=3 as suggested by the analysis leading to (3.8).[2] We see that the skirts of the mainlobes are wider than Fig. 3.2(a) and that the peak sidelobe levels are higher. This suggests that (3.8) is too conservative. Using the rule-of-thumb in equation (3.9) yields $M2 = 9$ and utilising this value results in the improved beampatterns of Fig. 3.2(c) which are highly reminiscent of the benchmark curves of Fig. 3.2(a).

Increasing D/λ to 0.5 and setting $M2 = 5$ as suggested by (3.8) yields the wide skirts and high sidelobes of Fig. 3.2(d), but increasing $M2$ to 11 as in (3.9) provides the acceptable results of Fig. 3.2(e).

Further increasing D/λ to 1.5 and $M2$ to 13 in accordance with (3.8) gives the borderline results in Fig. 3.2(f), whereas setting $M2 = 19$ from (3.9) yields the improved results of Fig. 3.2(g).

Finally, we show in Fig. 3.2(h) the results for $D/\lambda = 2.5$ with $M2 = 21$ from (3.8). The peak sidelobe levels are a little elevated and the sidelobe levels settle out at about -35dB. These results are again of borderline acceptability, but are improved as shown in Fig. 3.2(i) by increasing $M2$ to 27 in accordance with (3.9).

Summary

These experiments near broadside have demonstrated the utility of equation (3.9) in establishing the value of the length, $M2$, of the bend compensation filter, C(.).

3.4.2 Experiments near endfire

Given that the bend effect is a function of angle of arrival we now turn our attention to steering directions near endfire, e.g. near $\cos(\theta_0) = 0$, and we repeat the

[2] Actually, (3.8) yields $M2 = 2$ but in our simulations $M2$ is always odd.

previous series of experiments. In Ψ terms, with M=128 and f_c=1, endfire is at $\Psi = M/2 = 64$ and so we set the steering directions to Ψ_0 = 60, 60.1, 60.2, 60.3, 60.4, 60.5, with the corresponding s values ranging from 0 to 0.5.

We again start with the benchmark case of a linear array with no bend compensation, i.e. $D/\lambda = 0$, $M2$ =1. The results with $M1$=5 are shown in Fig. 3.3(a) which, it should be remarked, are identical to those in Fig. 3.2(a).

Increasing D/λ to 0.25 and using the rule-of-thumb in (3.9) to set $M2$ = 9 yields the results of Fig. 3.3(b), demonstrating effective bend compensation. Increasing D/λ further to 0.5 and setting $M2$ = 11 yields the acceptable results of Fig. 3.3(c).

However, increasing D/λ to 1.5 and 2.5 and using the rule-of-thumb values for $M2$ of 19 and 27, respectively, yields poorer results, as shown in Figs. 3.3(d) and 3.3(e). The reason for the inferior performance can be traced to the fact that $\Psi_0 \approx 60$ and hence lies only about 4 FFT cells from "endfire" (= $M/2$=64). Over a large number of similar experiments, it was observed that where the bend corrector's length of $M2$ is such that it overlaps much past the endfire cell (which occurs in our case if $M2 > 9$ (=2x4+1)) then the interpolation becomes compromised and the results are inferior. This certainly is the case for the latter two experiments with $M2$ = 19 and 27. In general the problem occurs if $M2/2 > M/2 - |\Psi_0|$, approximately, or

$$|\Psi_0| > M/2 - M2/2 \qquad (3.10)$$

The root cause of the problem is the fact that the bend effect is a function of cos(θ) and thus varies rapidly in the vicinity of endfire. There seems no simple solution to this difficulty.

It should be noted, however, that further experiments with the IBF and CBF beamformers, to be shown later, will demonstrate that the above problem also exists for the CBF. Hence it is not strictly a function of our IBF approach but is inherent to the CBF approach, itself.

Summary

The experiments near endfire reveal a potential bend-correction problem for the IBF using steering directions within about $M2/2$ FFT cells of endfire. Later experiments will demonstrate that this problem also exists for the CBF.

3.4.3 Experiments with $N/M \approx 0.5$

The foregoing experiments have all featured $N = M = 128$ and we now turn our attention to the case where the number of sensors, N, is less than the FFT length, M. The worst case, as discussed earlier, occurs where $N/M \approx 0.5$ so we set $N = 65$, $M = 128$ in the following experiments. Following (3.9) we expect that the values of $M1$ and $M2$ simply scale up by the ratio of M/N and this will be verified by the simulation results.

We re-run the near-broadside case, $\Psi_0 \approx 0$ with $D/\lambda = 0.5$. If we do not correct for the N/M ratio and use the previous values of $M1=5$, $M2 = 11$ we get the results of Fig. 3.4(a) which are inferior. However, the problems are ameliorated on scaling by M/N, as indicated in (3.9), such that $M1 = 9$, $M2 = 23$ (recall that $M1$, $M2$ are odd in our simulations), yielding the improved results in Fig. 3.4(b).

The near-endfire results (not shown for space reasons) show the same requirement for the use of (3.9), including the M/N factor, but it should be noted that the near-endfire problems alluded to above are worsened by the necessary increase in $M2$.

3.4.4 Some plots of the bend correction filter, $C(p,\theta_0)$.

Before moving on to further beamforming experiments, it might be useful to look at a few plots of the magnitude of the correction filter function, $|C(p,\theta_0)|$, to see how it varies with some of the experimental parameters. We use a near-broadside case, $\Psi_0 = 0.5$ (see footnote [3]) with $M1$=5 and N=M=128. We have four values of D/λ {=0.25, 0.5, 1.5 , 2.5} and use the four corresponding values of $M2$ {=9, 11, 19, 27}from (3.9). The four length-$M2$ plots of $|C(p,\theta_0)|$ vs. p are shown in Figs. 3.5(a-d) where the index p runs along the x-axis[4]. It might be remarked that Figs. 3.5(c) and (d) suggest that the length of $M2$ might be a little conservative as there appears to be some truncation of $C(p,\theta_0)$. However, our previous results suggest that this does not seem to translate into a serious performance problem.

If we choose the near-endfire case of $\Psi_0 = 60.5$ and re-run the case with D/λ = 2.5, then the results of Fig. 3.6, when compared to those of Fig. 3.5(d), reveal that the $C(p,\theta_0)$ function "narrows" as endfire is approached, $|\cos(\theta_0)| \to 0$, and the $M2$=27 value now seems pessimistic. However, this is mitigated by the simplicity of (3.9).

Finally we examine the near-broadside case where D/λ is reduced to 0.5 and N is also reduced to 65. According to (3.9), $M2$ is approximately 23 and this is the result plotted in Fig. 3.7. Again we note some evidence of minor truncation. However, overall we have more evidence of the utility of (3.9).

3.5 Simulation experiments over 0-360^0

The foregoing IBF experiments have been performed in Ψ-space with the appropriate bend correction utilised. However, it has not addressed the issue of a source

[3] The relationship between θ and Ψ is given in (2.5).
[4] To be more precise, the p-axis labelling should run from -(M2-1)/2 to +(M2-1)/2 rather than 1 to M2.

sharing the same Ψ value but on the "wrong" side of the array, where the phase errors due to the bend have the opposite sign. Hence, to fully understand the interpolation beamformer's action we need to plot beampatterns over the full 0-360^0 range. We shall revisit some of our earlier experiments and re-run them in this light.

We start by setting D/λ=1.5, f_c =1, $M1$=5, $M2$=19. We choose N=M=64 so that than the IBF beampattern is sufficiently wide to enable some detail to be visible in the polar plot of Fig. 3.8. The IBF is steered to $\theta_0 = 20^0$ where we observe a relatively narrow beam with close-in sidelobes levels at -30dB with respect to the peak. [Note that the beampattern is normalised to the vicinity of 50dB maximum for plotting purposes; the annular rings represent 10dB increments]. The response in the vicinity of the complementary angle of 160^0 is clearly visible and while its peak is some 10dB below the steered output, the broadness of the complementary response is of concern.

Also on Fig. 3.8 we plot the benchmark CBF beampattern for the same bent array. The two curves are barely distinguishable by eye and so we plot the difference in the two beampatterns (difference = IBF-CBF where IBF and CBF represent beampatterns expressed in dB) and superimpose it on the 40dB contour for convenience. Both beampatterns are normalised by the maximum output of the CBF (itself set at 50dB) and beampowers less than 0dB are set to 0dB to avoid extraneous detail in the difference plot. The difference curve shows that there are negligible performance differences in the major lobe areas. Those larger differences that do exist occur where the sidelobe levels are sufficiently low for these to be of no concern.

Finally we note that the SNR loss associated with the IBF (loss = SNR(IBF)-SNR(CBF) where both are in dB), computed via equations (3.10), (3.11), is about -0.01dB as indicated in the upper right of the figure.

Reducing the bow value to D/λ = 0.5 produces the results of Fig. 3.9. The polar plot shows that the beampatterns in the vicinity of the steering direction of 20^0 are largely

unaffected while the complementary responses are considerably narrower, both as expected. Again we note little meaningful difference in the IBF and CBF beampatterns and little SNR loss.

In Fig. 3.10 we increase M and N to 128 and set the steering direction to $\theta_0=66^0$. We have a significant bow value of $D/\lambda=2.5$ and (3.9) suggests $M1=5$ and $M2=27$ as suitable filter lengths for the IBF. On the polar plot of Fig. 3.10 we again note a broad and relatively high complementary beam. There is also a response in the opposite endfire vicinity which exceeds the -30dB level. Again we note that there is little substantive difference in the performance of the IBF and CBF beampatterns.

Reducing the bow to $D/\lambda=1.5$ with the concomitant reduction in $M2$ to 19 improves matters as shown in Fig. 3.11. A further reduction in bow to $D/\lambda=0.5$ with $M2=11$ yields the plots in Fig. 3.12. In this case the bow does not present a particular challenge and the each beamformer's performance is close to that of a linear array.

In Fig. 3.13 we show the case where $D/\lambda=1.5$ but the frequency ratio is set to $f_r=0.5$. The salient feature here, with a steering direction of 60^0, is the absence of any response near the opposite endfire. These results should be compared to Fig. 3.10.

In Fig. 3.14 we steer to 45^0 with a bow of $D/\lambda=0.5$. The number of sensors, N, is reduced to 65 (with the FFT length, M, retained at 128). If we do not compensate for the M/N ratio and retain $M1 = 5$ and $M2 = 11$, then the results of Fig. 3.14 indicate an unacceptable increase in the sidelobe levels near the steering direction for the IBF. Increasing $M1$, $M2$ in accordance with (3.9) to $M1=9$, $M2=21$ generates the improved results of Fig. 3.15. We note again in Fig. 3.15 that the IBF and CBF results are similar.

3.6 Summary

We have demonstrated that interpolation beamforming of a bent array is feasible and have established working guidelines for the choice of the two critical filter lengths, *M1* and *M2*. The SNR performance of the interpolation beamformer has been shown to be within about 0.1dB of the benchmark conventional, delay-and-sum beamformer.

The interpolation beamformer and the conventional beamformer exhibit very similar problems associated with (i) the broadening of the complementary lobe and (ii) the loss of performance where the steering direction is close to endfire. The latter problem is common to any line-array beamformer operating near endfire.

Overall, an interpolation beamformer designed on the basis of the guidelines introduced in this report offers bent-array beamforming performance which is almost indistinguishable from that of the underlying, brute-force conventional beamformer

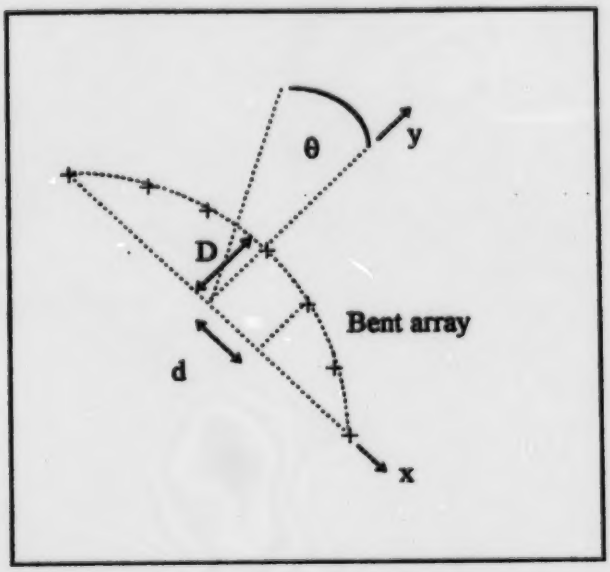

Fig 3.1 Geometry of the bent array. The bend takes the form of an arc of a circle with the unbent line array as a chord. The diagram is exaggerated for effect.

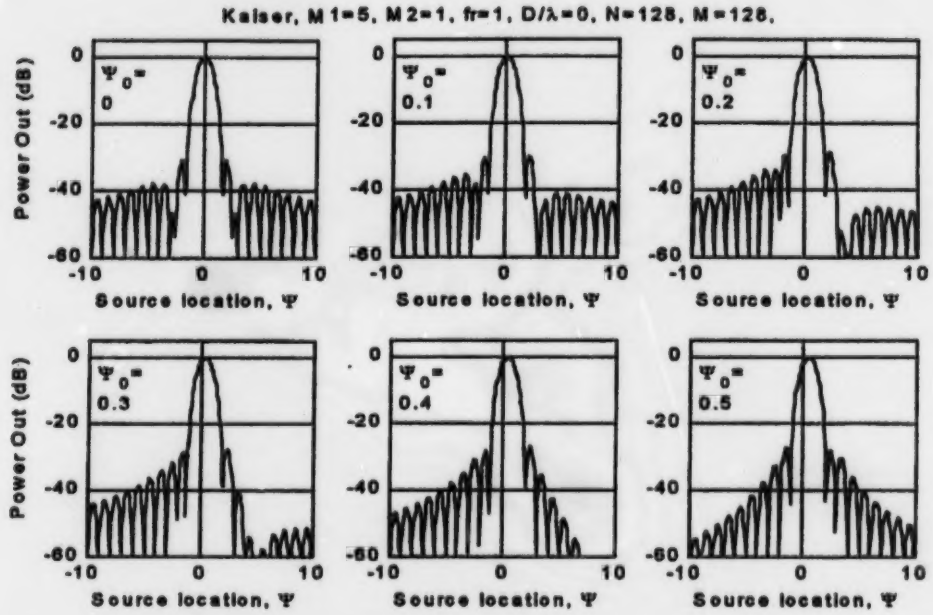

Fig. 3.2(a) Interpolation beamformer output near broadside.
$D/\lambda = 0, M1=5, M2=1, f_r=1, N=M=128$

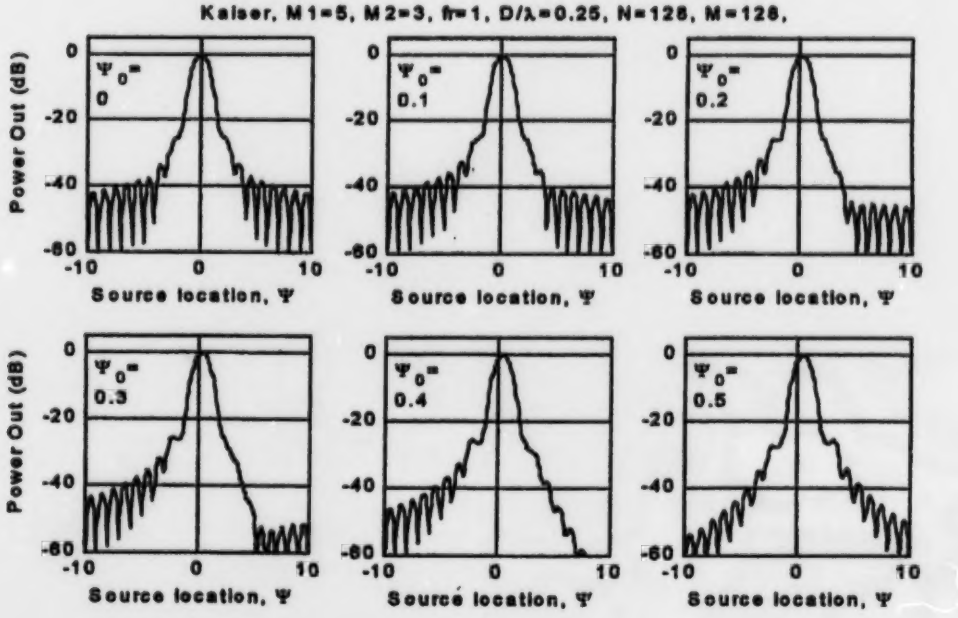

Fig. 3.2(b) Interpolation beamformer output. $D/\lambda = 0.25, M1=5, M2=3, f_r=1, N=M=128$

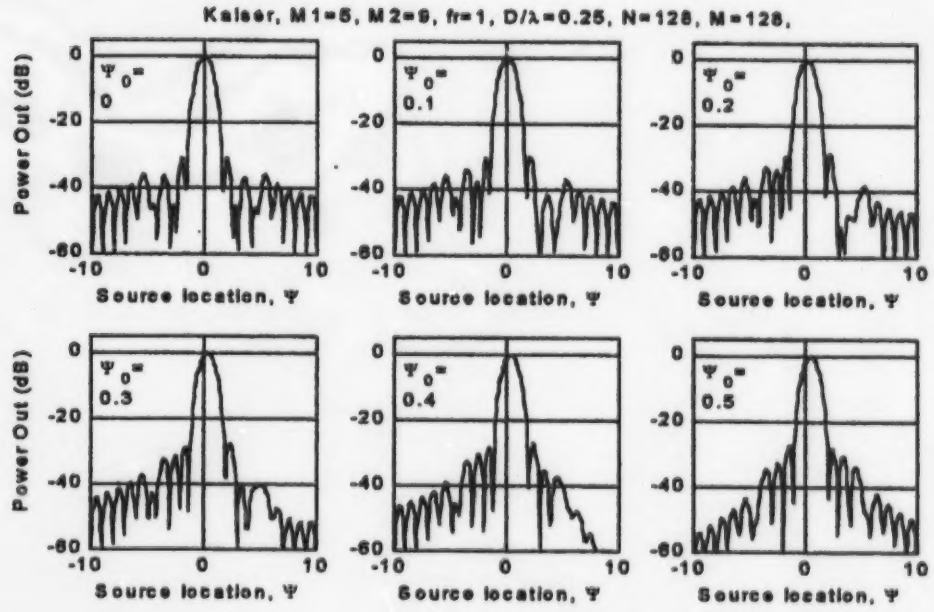

Fig. 3.2(c) Interpolation beamformer output. $D/\lambda = 0.25$, $M1$=5, $M2$=9, f_r=1, N=M=128

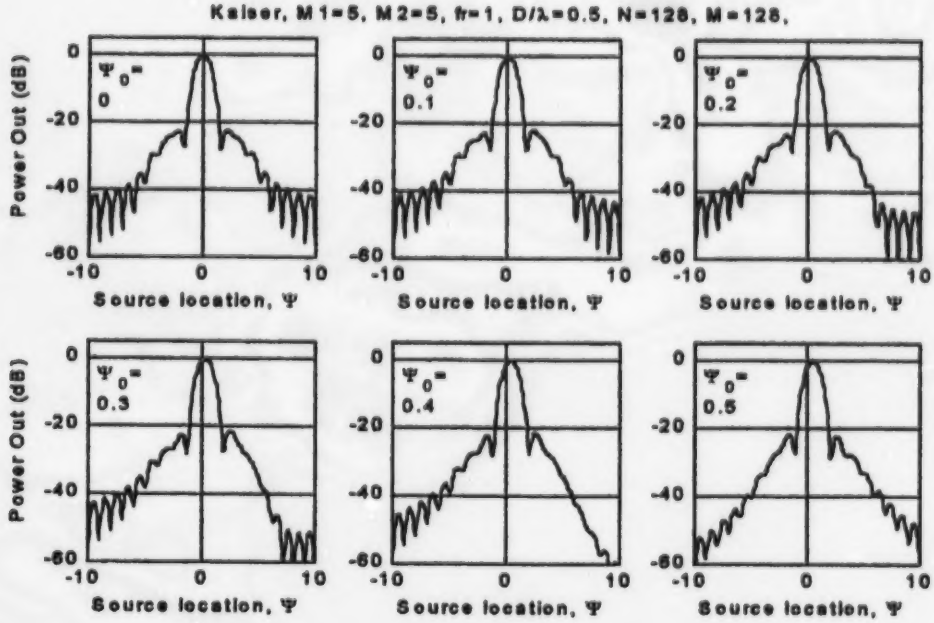

Fig. 3.2(d) Interpolation beamformer output. $D/\lambda = 0.5$, $M1$=5, $M2$=5, f_r=1, N=M=128

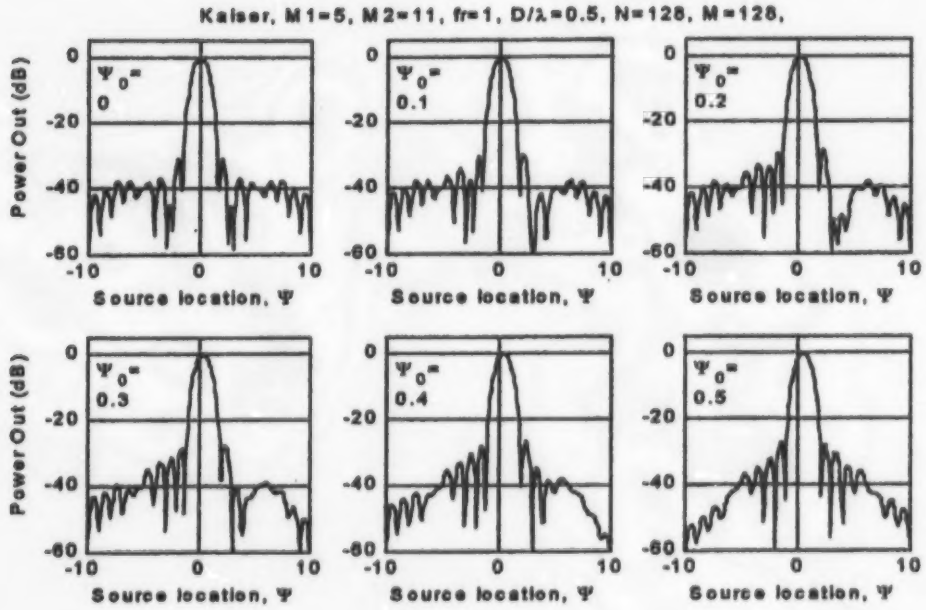

Fig. 3.2(e) Interpolation beamformer output. $D/\lambda = 0.5$, $M1$=5, $M2$=11, f_r=1, N=M=128

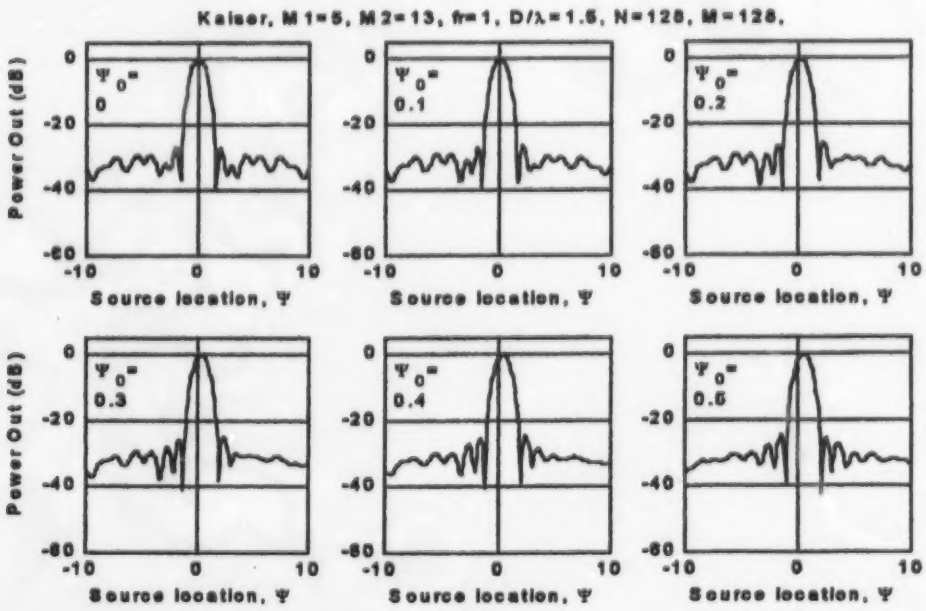

Fig. 3.2(f) Interpolation beamformer output. $D/\lambda = 1.5$, $M1$=5, $M2$=13, f_r=1, N=M=128

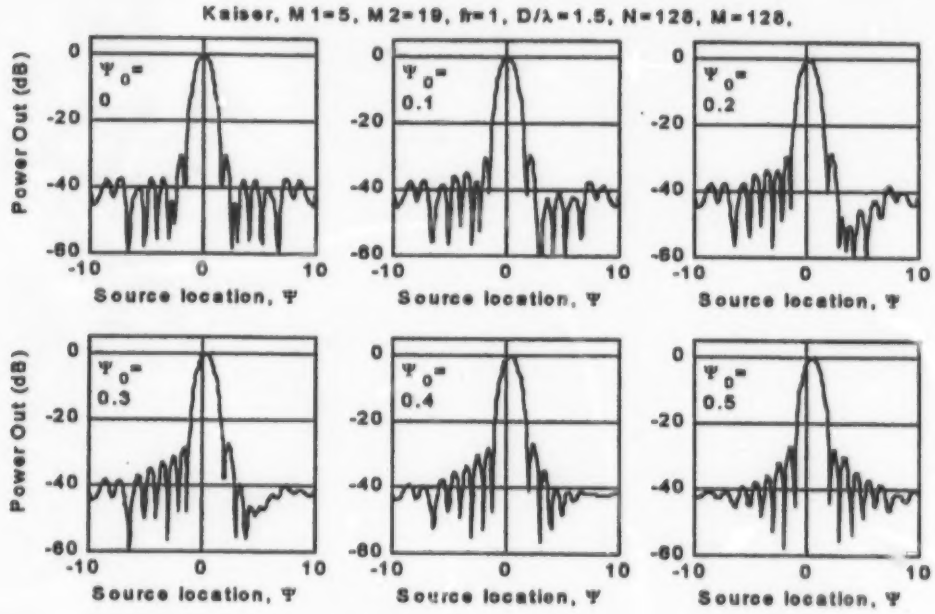

Fig. 3.2(g) Interpolation beamformer output. $D/\lambda = 1.5$, $M1$=5, $M2$=19, f_r=1, N=M=128

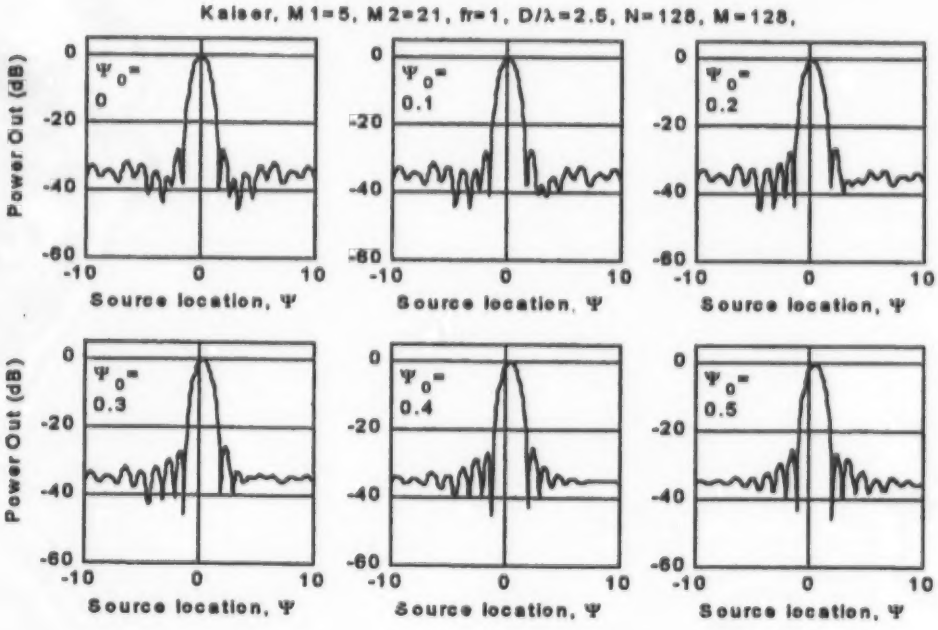

Fig. 3.2(h) Interpolation beamformer output. $D/\lambda = 2.5$, $M1$=5, $M2$=21, f_r=1, N=M=128

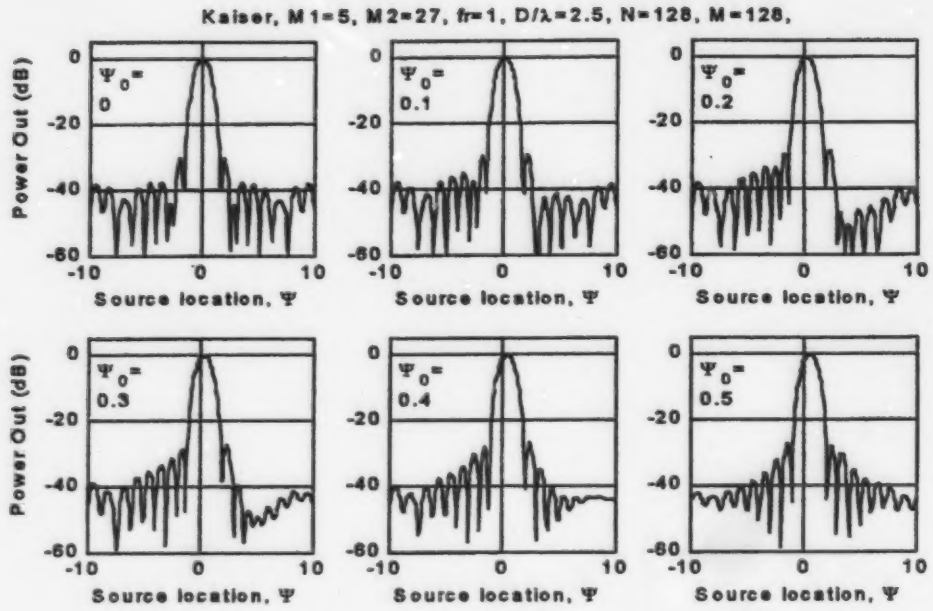

Fig. 3.2(i) Interpolation beamformer output. $D/\lambda = 2.5$, $M1$=5, $M2$=27, f_r=1, N=M=128

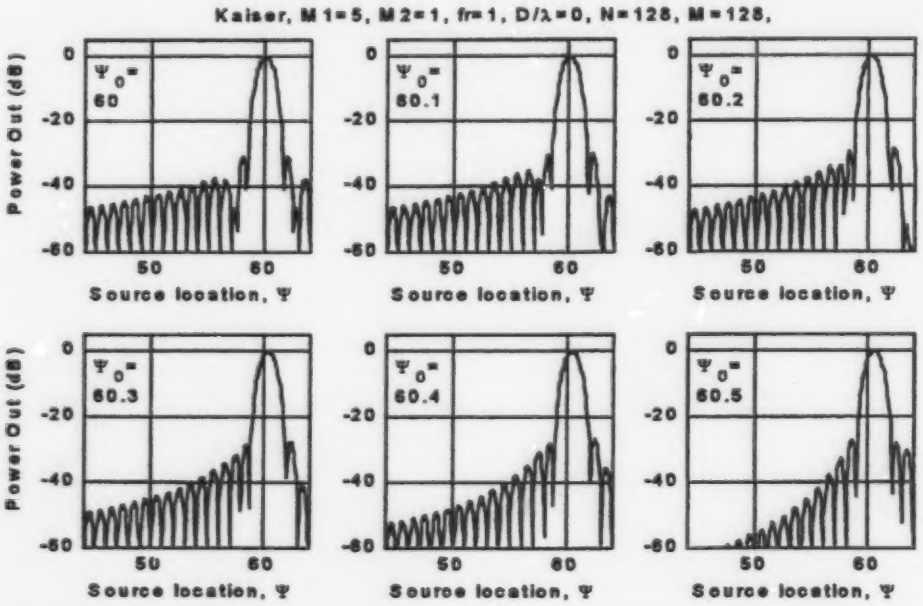

Fig. 3.3(a) Interpolation beamformer output near endfire.
$D/\lambda = 0$, $M1$=5, $M2$=1, f_r=1, N=M=128.

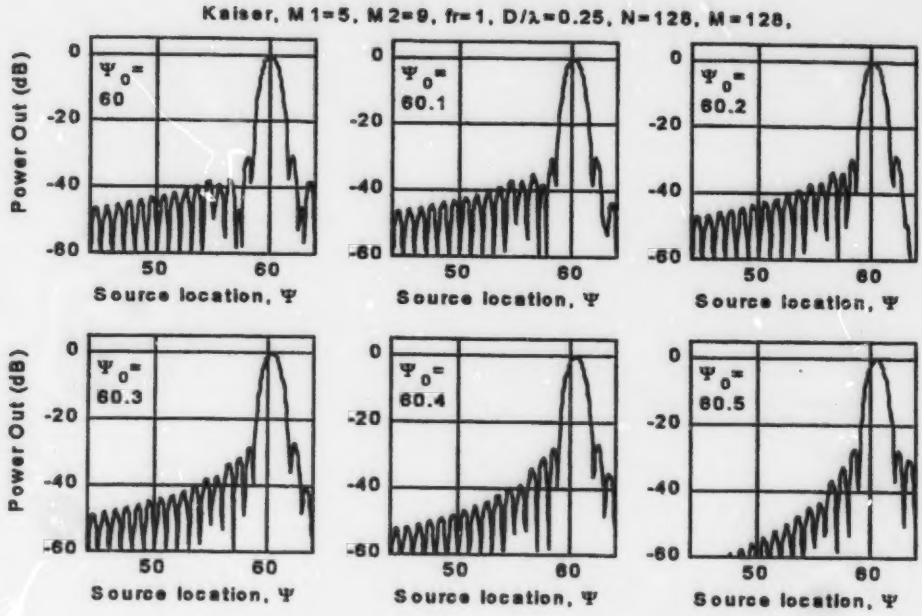

Fig. 3.3(b) Interpolation beamformer output. $D/\lambda = 0.25$, $M1$=5, $M2$=8, f_r=1, N=M=128

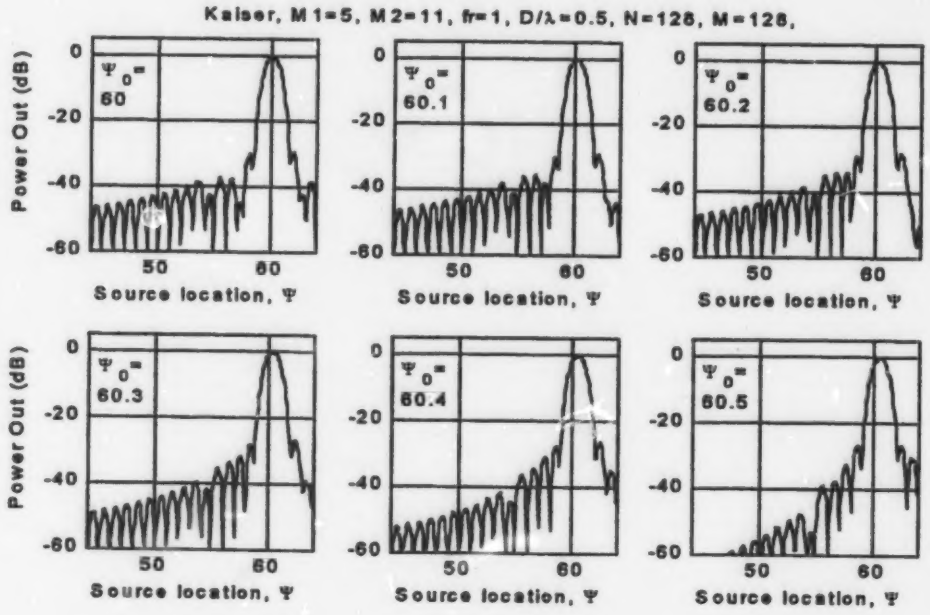

Fig. 3.3(c) Interpolation beamformer output. $D/\lambda = 0.5$, $M1$=5, $M2$=11, f_r=1, N=M=128

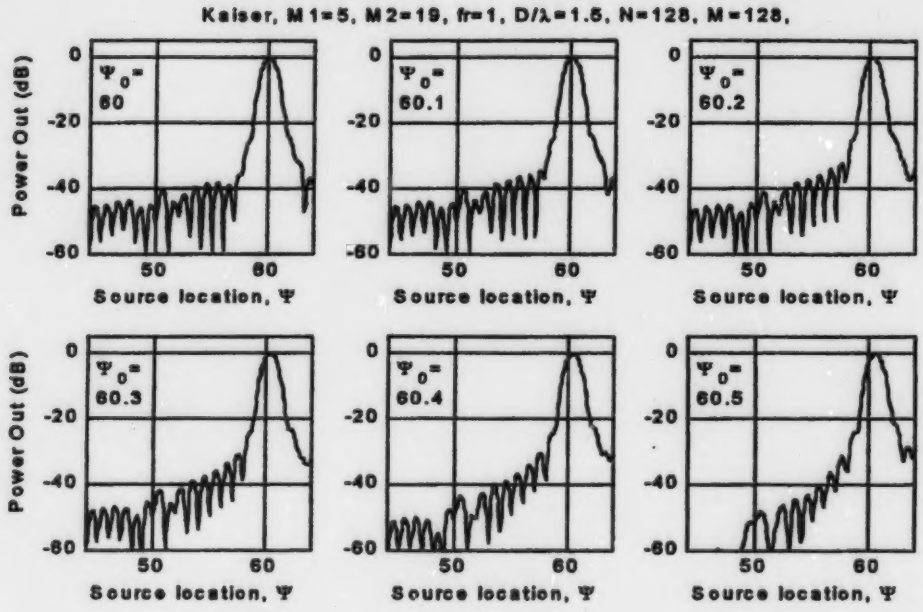

Fig. 3.3(d) Interpolation beamformer output. $D/\lambda = 1.5$, $M1$=5, $M2$=19, f_r=1, N=M=128

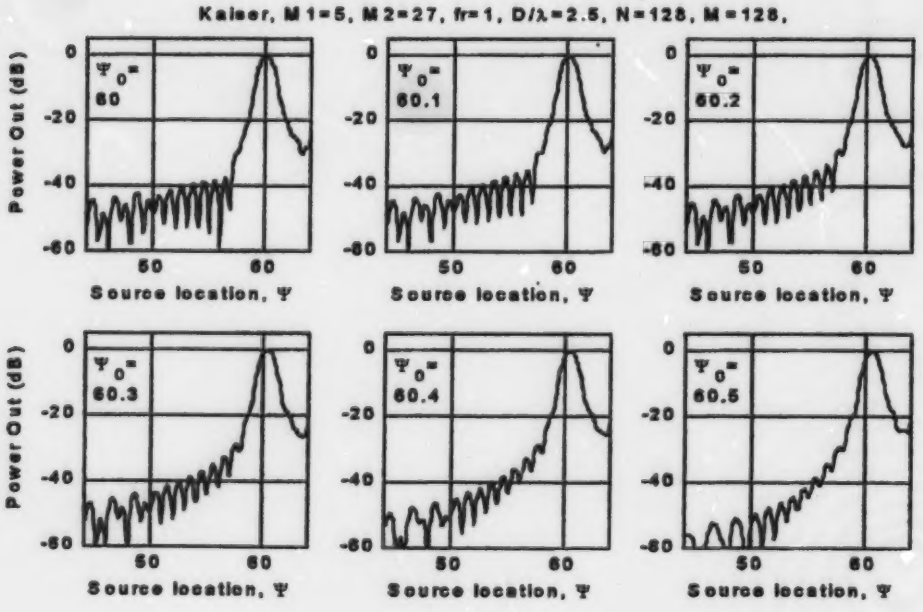

Fig. 3.3(e) Interpolation beamformer output. $D/\lambda = 2.5$, $M1$=5, $M2$=27, f_r=1, N=M=128

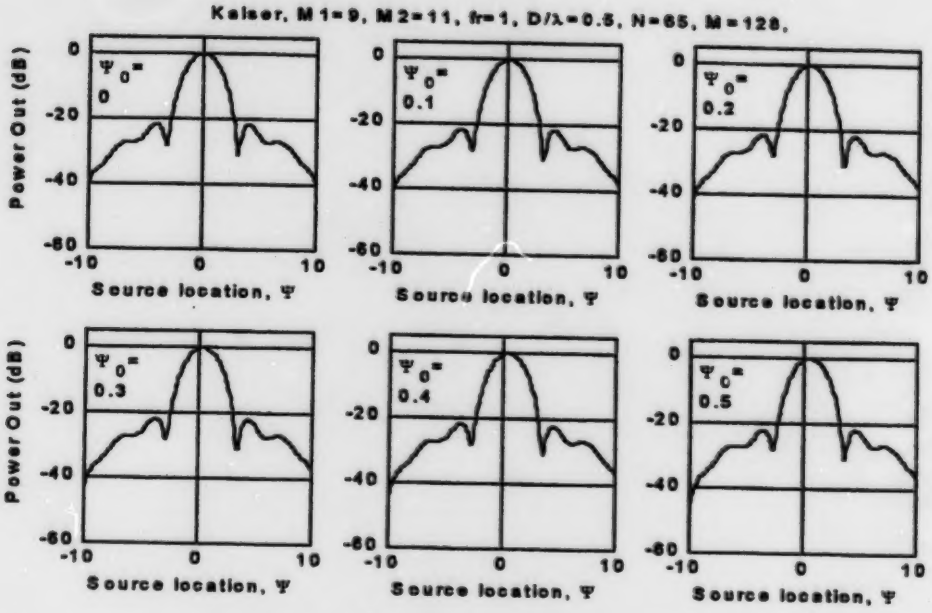

Fig. 3.4(a) Interpolation beamformer output. D/λ = 0.5, $M1$=9, $M2$=11, f_r=1, N=65, M=128.

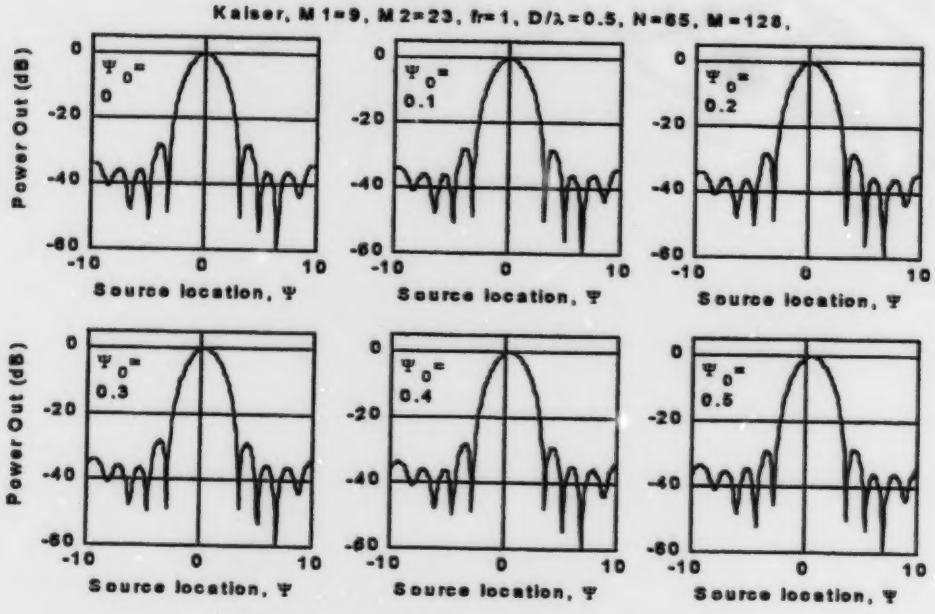

Fig. 3.4(b) Interpolation beamformer output. D/λ = 0.5, $M1$=9, $M2$=23, f_r=1, N=65, M=128.

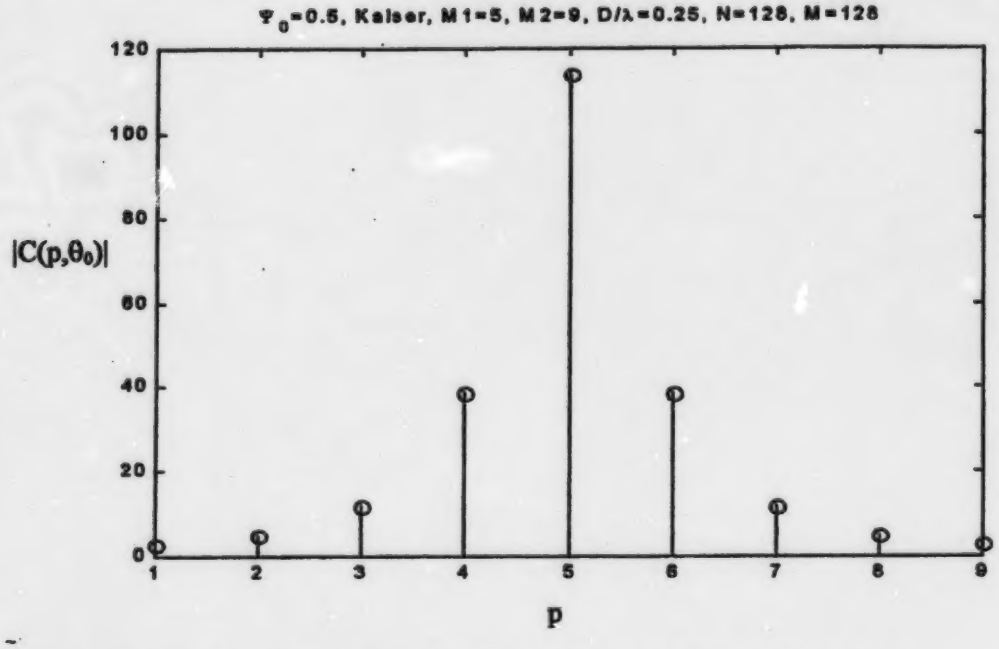

Fig. 3.5(a) Bend correction filter, $|C(p,\theta_0)|$. Ψ_0 =0.5, $D/\lambda = 0.25$, $M2 = 9$.

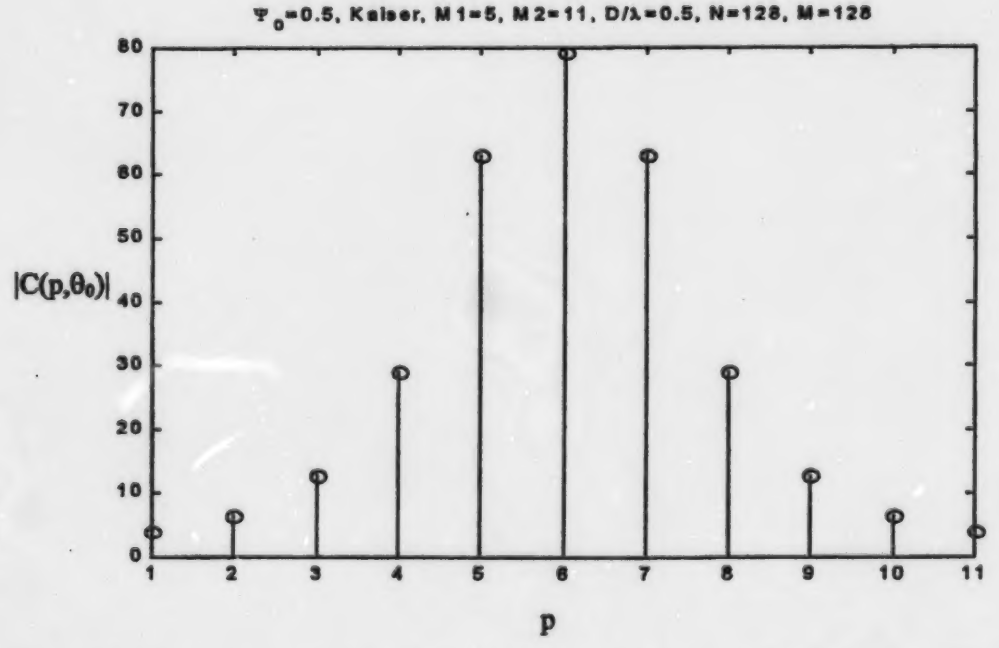

Fig. 3.5(b) Bend correction filter, $|C(p,\theta_0)|$. Ψ_0 =0.5, $D/\lambda = 0.5$, $M2$ =11.

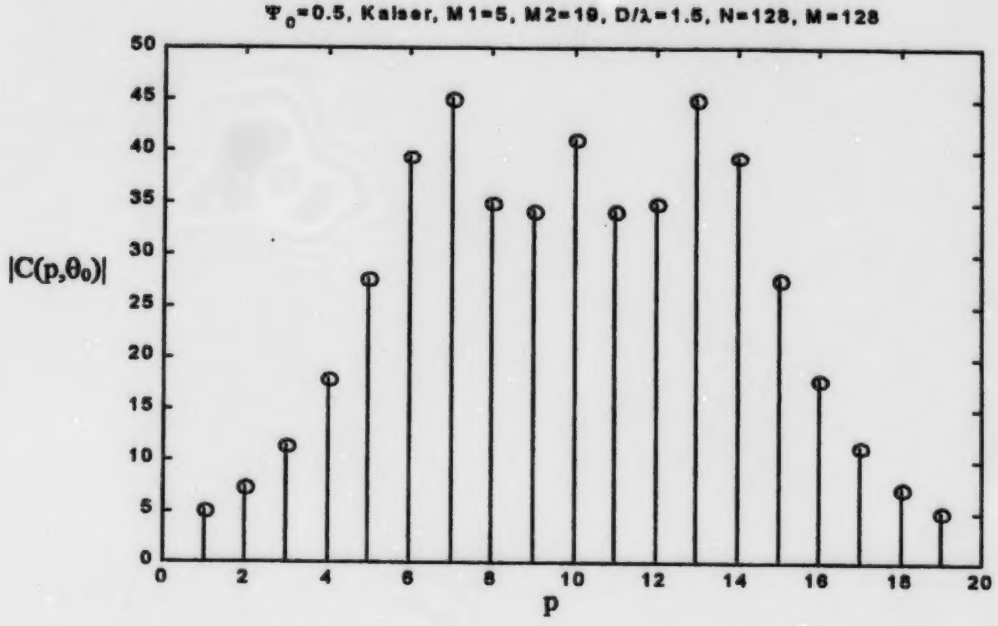

Fig. 3.5(c) Bend correction filter, $|C(p,\theta_0)|$. Ψ_0 =0.5, $D/\lambda = 1.5$, $M2 = 19$.

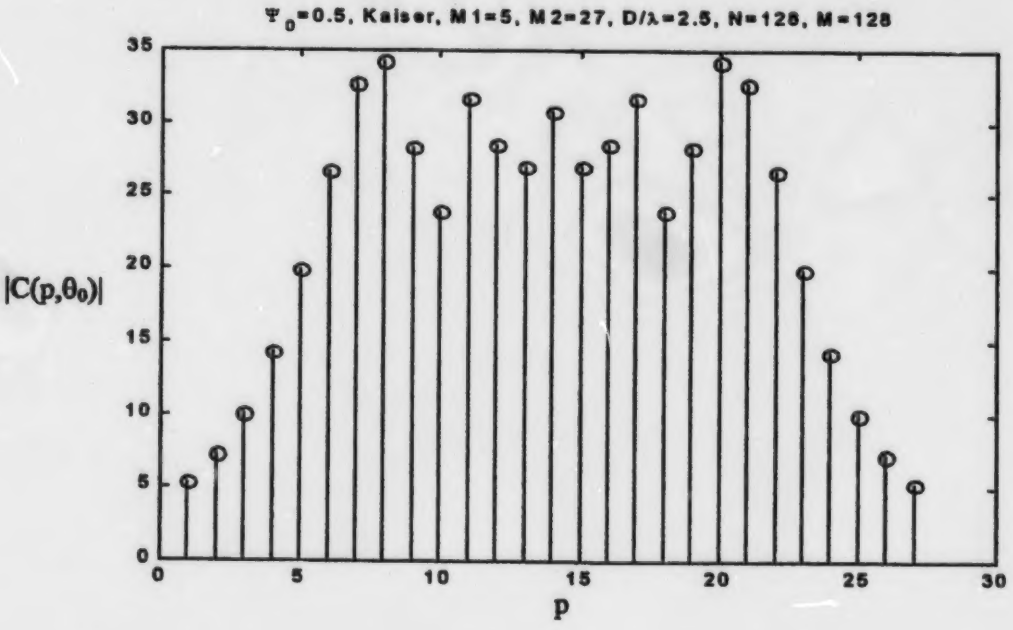

Fig. 3.5(d) Bend correction filter, $|C(p,\theta_0)|$. Ψ_0 =0.5, $D/\lambda = 2.5$, $M2 = 27$.

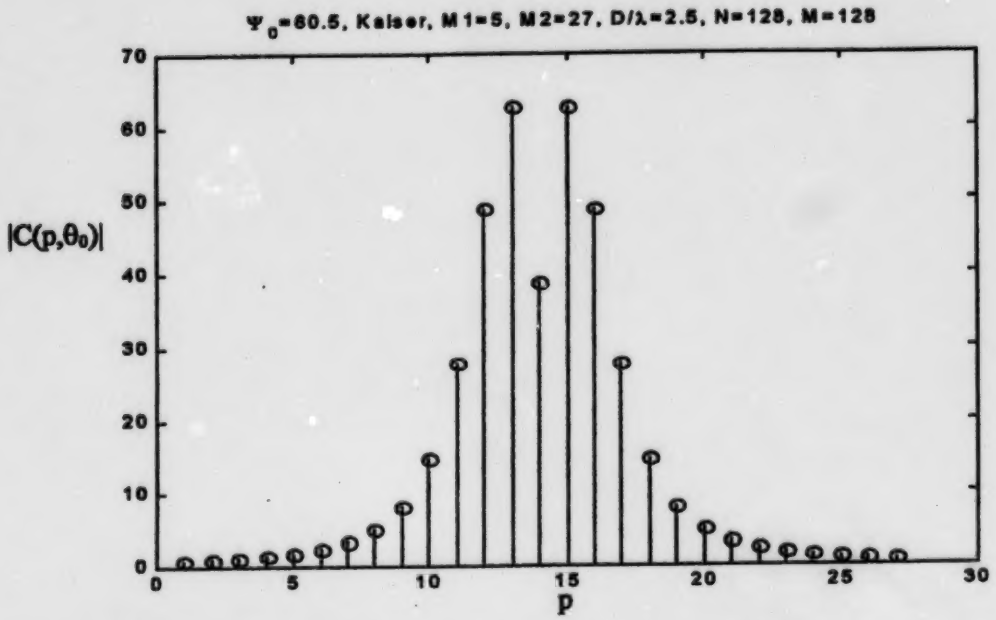

Fig. 3.6 Bend correction filter, $|C(p,\theta_0)|$. Ψ_0 =60.5, $D/\lambda = 2.5$, $M2 = 27$.

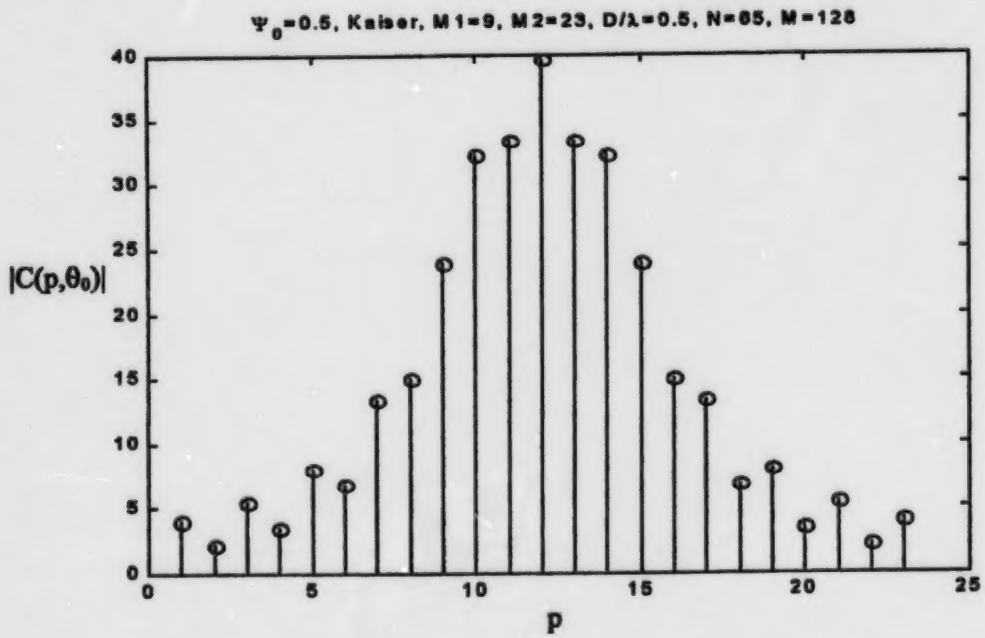

Fig. 3.7 Bend correction filter, $|C(p,\theta_0)|$. Ψ_0 =0.5, $D/\lambda = 0.5$, $M2 = 23$, N=65, M =128

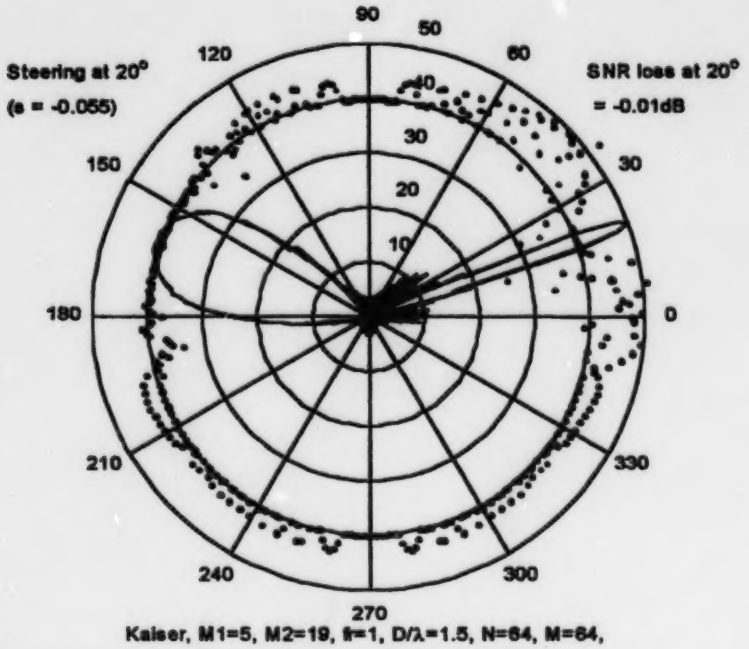

Fig. 3.8 Beampatterns of IBF and CBF. Difference shown as •••.
$\theta_0 = 20^0$, $D/\lambda = 1.5$, $M1$=5, $M2$=19, $f_r = 1$, N=64, M=64.

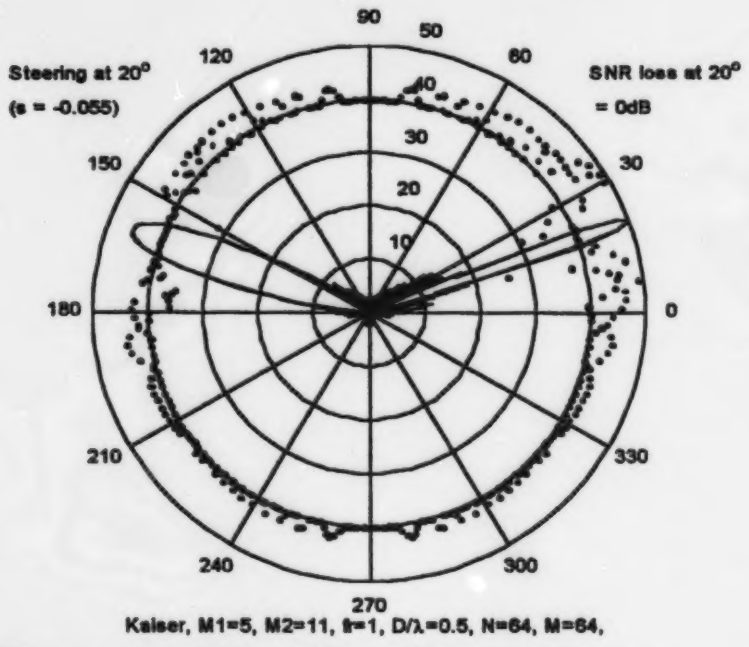

Fig. 3.9 Beampatterns of IBF and CBF. Difference shown as •••.
$\theta_0 = 20^0$, $D/\lambda = 0.5$, $M1$=5, $M2$=11, $f_r = 1$, N=64, M=64.

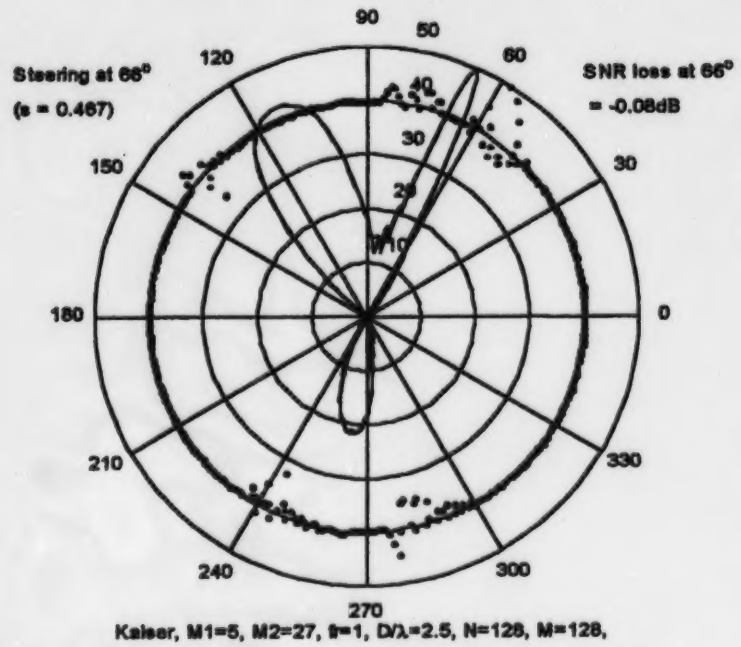

Fig. 3.10 Beampatterns of IBF and CBF. Difference shown as •••.
$\theta_0 = 66^0$, $D/\lambda = 2.5$, $M1$=5, $M2$=27, $f_r = 1$, N=128, M=128.

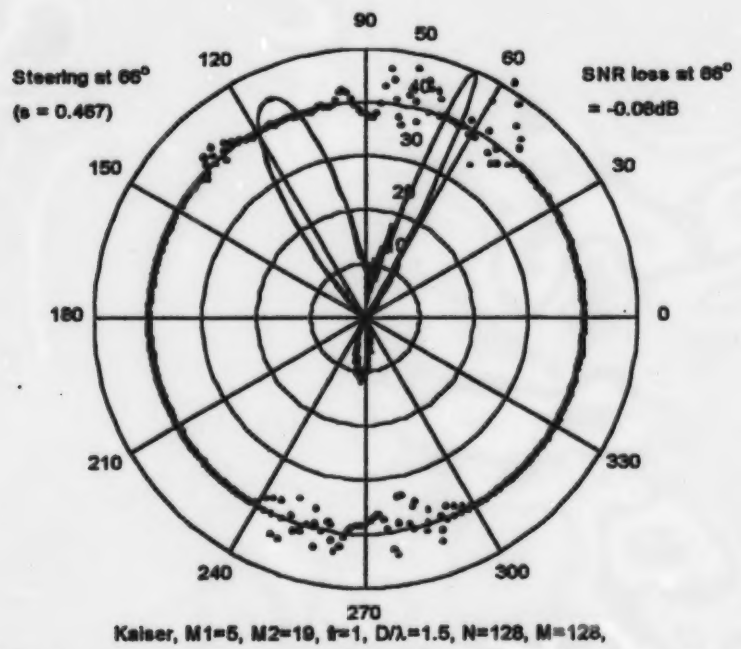

Fig. 3.11 Beampatterns of IBF and CBF. Difference shown as •••..
$\theta_0 = 66^0$, $D/\lambda = 1.5$, $M1$=5, $M2$=19, $f_r = 1$, N=128, M=128.

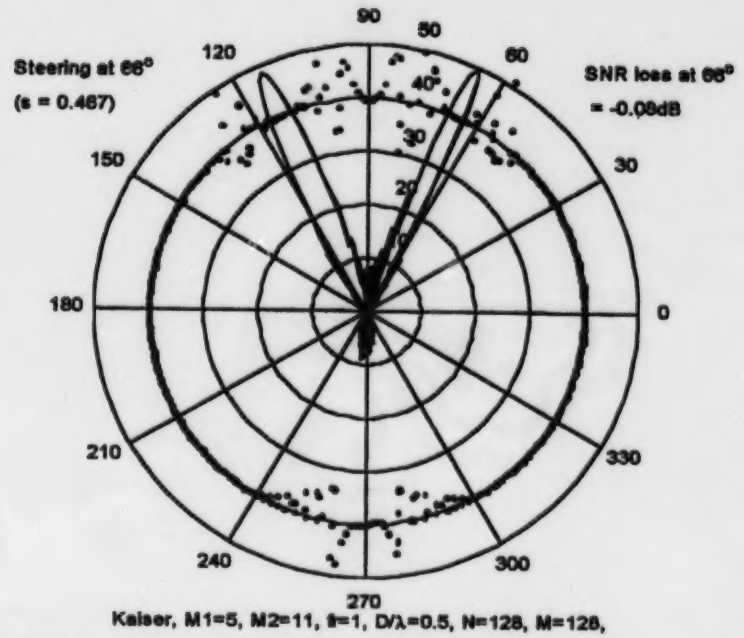

Fig. 3.12 Beampatterns of IBF and CBF. Difference shown as ooo.
$\theta_0 = 66^0$, $D/\lambda = 0.5$, $M1$=5, $M2$=11, $f_r = 1$, N=128, M=128.

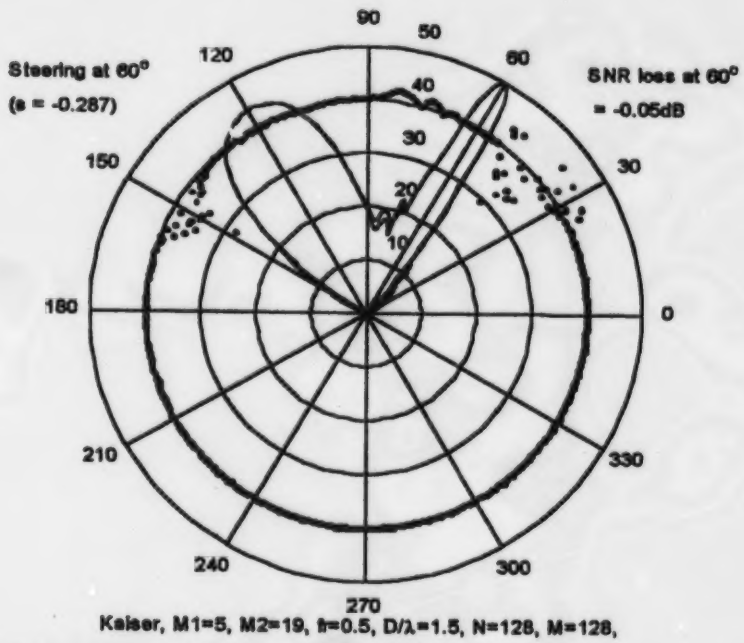

Fig. 3.13 Beampatterns of IBF and CBF. Difference shown as ooo.
$\theta_0 = 60^0$, $D/\lambda = 1.5$, $M1$=5, $M2$=19, $f_r = 0.5$, N=128, M=128.

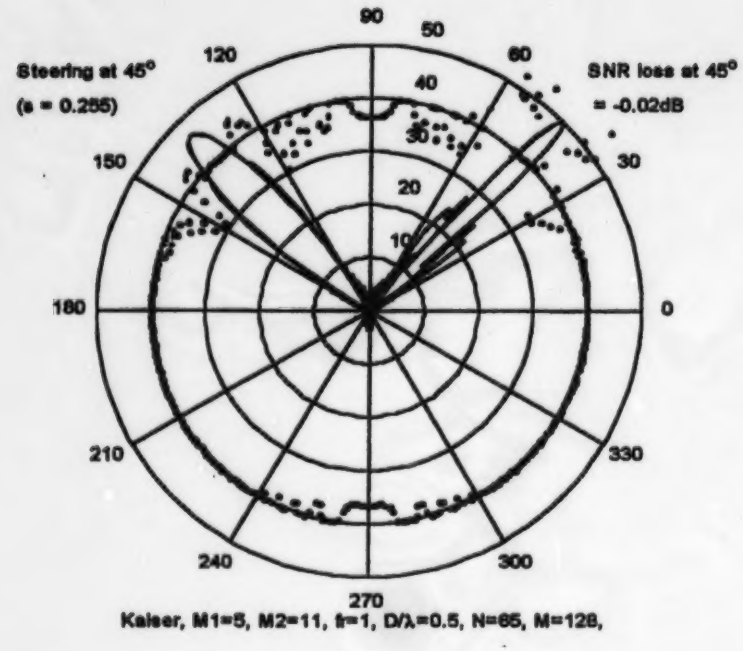

Fig 3.14 Beampatterns of IBF and CBF. Difference shown as •••.
$\theta_0 = 45^0$, $D/\lambda = 0.5$, $M1$=5, $M2$=11, $f_r = 1$, N=65, M=128.

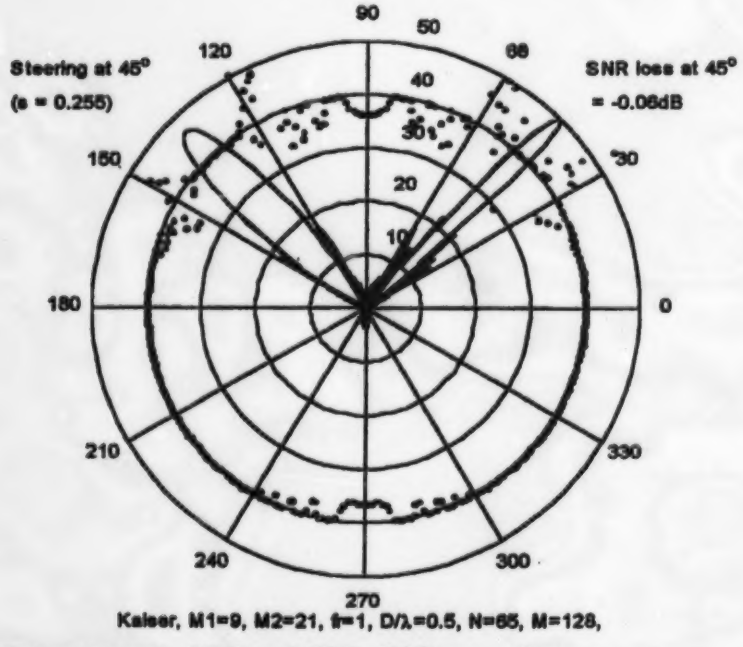

Fig 3.15 Beampatterns of IBF and CBF. Difference shown as •••.
$\theta_0 = 45^0$, $D/\lambda = 0.5$, $M1$=9, $M2$=21, $f_r = 1$, N=65, M=128.

4. Interpolation beamforming for an active sonar.

4.1 Introduction

In the previous section, we examined the interpolation beamformer's performance in terms of tonal signals impinging on a bent array. In an active sonar application, however, the signals of interest may well be wideband. In the examples to be presented here we assume linear FM chirps.

The simulations are based on MATLAB code written for a previous DREA report [4-1] and involve the following basic steps:

(i) Simultaneously record a time-series snapshot of L samples at each of the N sensors.

(ii) Take an L-point FFT of each sensor snapshot.

(iii) Extract the N Fourier coefficients at frequency f_i.

(iv) Choose a steering (or beam) direction and use the interpolation beamformer weights acting on the Fourier coefficients, as described earlier, to estimate the true Fourier coefficient for the signal component (if any) at this frequency and beam angle. Call this value a_i.

(v) Repeat (iii-iv) for all frequencies over the band of interest.

(vi) Perform an M-point inverse FFT on the $\{a_i\}$ data, zero-padded if necessary. This represents the wideband output time series from the beamformer for this snapshot at this beam angle.

(vii) This output time-series is concatenated with those from previous snapshots at the same beam angle and passed through a matched filter (correlation detector). For a properly designed system, the correlator response to the signal of interest is expected to be a narrow "spike" of duration much less than M samples, even though the signal of interest may well have a duration much greater than M.

4.2 Simulation results

We use a linear FM chirp as the signal of interest. The frequency sweeps from 313Hz to 375Hz over a duration of 500 samples. The sampling rate is 1kHz and there are M=128 samples per snapshot. The processing bandwidth is chosen as 280 to 400Hz. The array is a 64-element uniform array with an inter-element spacing of 1.88m. Acoustic propagation speed is assumed to be 1500m/s.

We use two chirps in our experiment. The first has an amplitude (measured at the sensor) of 0.13, originates from bearing 22^0 and has an arrival time commencing at sample number 245. The second has an amplitude of 0.33, originates from bearing 43.4^0 and has arrival time commencing at sample number 325. The uncorrelated background noise level, also measured at the sensor, has a standard deviation of 0.5.

The expected response to each chirp is a sinc-like function who mainlobe width is about $(375\text{-}313)^{-1}$s or about 15 time samples. Note that the difference in time of arrival, 80 samples, is quite large in terms of the expected response width (15 samples) but quite small in terms of the chirp duration (500 samples).

We examine the correlator outputs for a set of beams equi-spaced in $\sin(\theta)$-space. In Fig. 4.1 we have the correlator outputs for a basic Hamming-shaded beamformer where

there is no array curvature. This provides a benchmark for later results. We note two well-defined, sinc-like peaks at the expected times in the beams at 22 and 43.4^0 with negligible spill-over into adjacent beams.

In Fig. 4.2 we have the corresponding output where the array is bent with a maximum bow of 10m (about 2.67 wavelengths at the upper processing frequency of 400Hz). Due to the curvature, the Hamming-shaded beamformer now produces significant responses in multiple beams. There is no bend correction applied here.

In Fig. 4.3 we apply the interpolation beamformer (with Hamming shading) to the bent array. The filter lengths are $M1$=7 and $M2$=29 in accordance with our previous work. We note that the output peaks are well localised in the beams at 22^0 and 43.4^0 as desired. Indeed Fig. 4.3 compares quite favourably with the benchmark results of Fig. 4.1.

Finally, we show, in Fig. 4.4, the interpolation beamformer output for the bent array case where the chirp at 43.4^0 is replaced by one at the complementary, or conjugate, angle of (approximately) 137^0. We note that there is a lower-level, though still significant (and undesirable) response in the beam at 43.4^0 and in at least nine adjacent beams. This result is in accordance with our previous observations concerning the spatially broad response to a signal at or near the conjugate angle.

4.3 Summary

We have demonstrated that the interpolation beamformer may be applied to an active sonar scenario. However, there remains the problem of the undesirable response to signals at or near conjugate bearings. As mentioned earlier, this is not a problem unique to the interpolation beamformer, but one which is inherited from the underlying "delay and sum" approach.

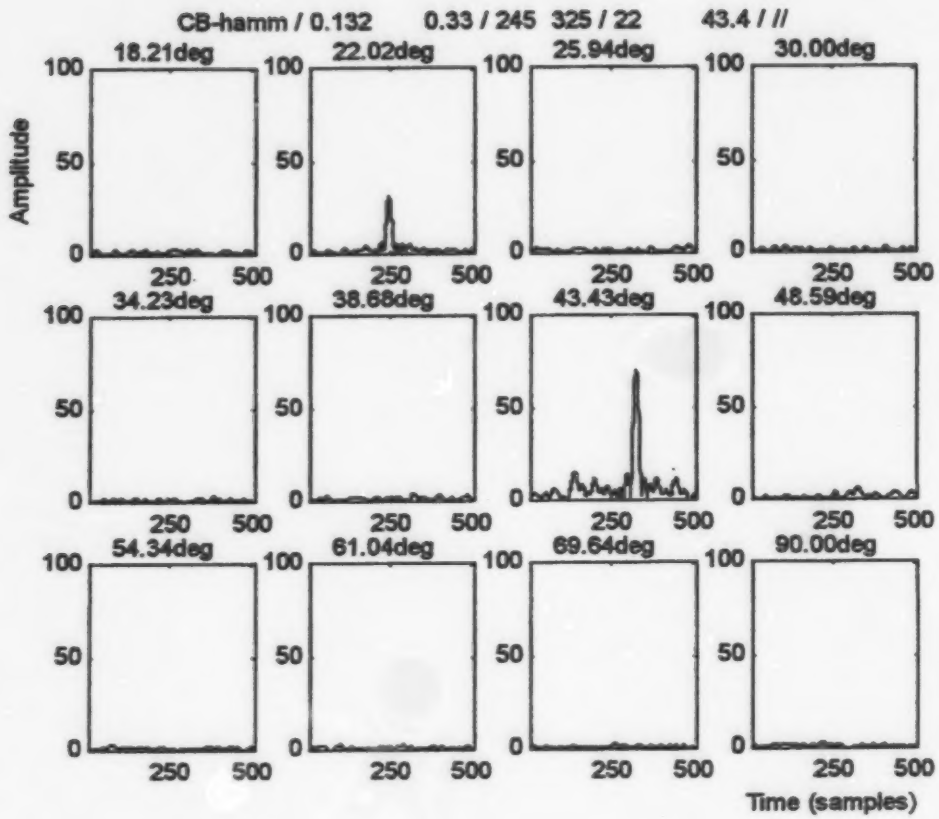

Fig. 4.1 Correlator output for WB Hamming -shaded beamformer. Unbent line array.

Two chirp sources: Stronger at 43.4^0, arrival time at sample 325; weaker at 22^0, arrival time at sample 245. Linear chirp sweep from 313 to 375Hz over duration of 500 samples. 64 sensors. Spacing d=1.88m. Processing band 280-400Hz. Sampling rate 1kHz. Snapshot length 128 time samples. 12 beams.

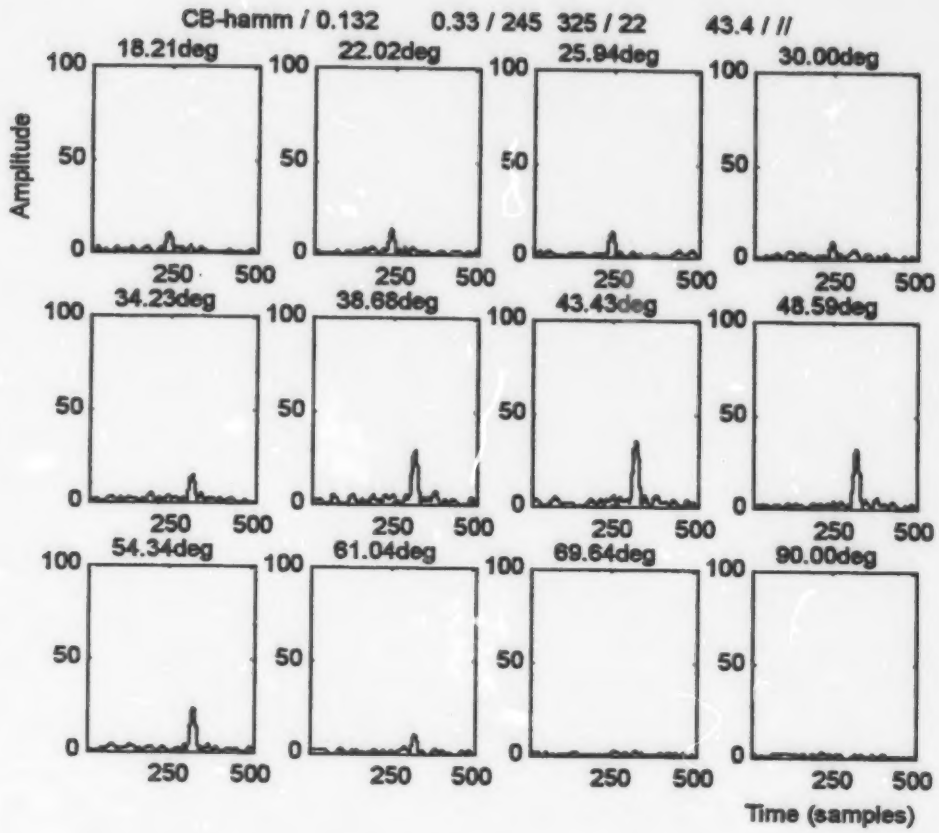

Fig. 4.2 Correlator output for WB Hamming-shaded beamformer. Bent line array. Bow = 10m.

Two chirp sources: Stronger at 43.4^0, arrival time at sample 325; weaker at 22^0, arrival time at sample 245. Linear chirp sweep from 313 to 375Hz over duration of 500 samples. 64 sensors. Spacing d=1.88m. Processing band 280-400Hz. Sampling rate 1kHz. Snapshot length 128 time samples. 12 beams.

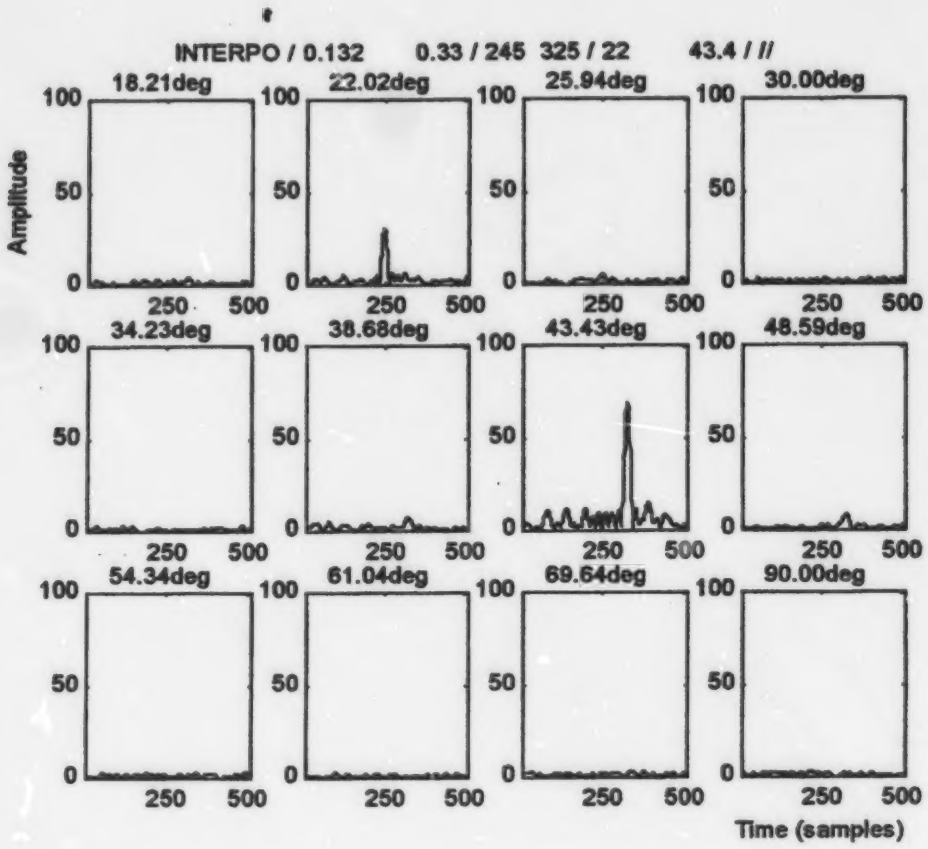

Fig. 4.3. Correlator output for WB Interpolation beamformer. Bent line array. Bow = 10m. Compare with Fig. 4.1

Two chirp sources: Stronger at 43.4^0, arrival time at sample 325; weaker at 22^0, arrival time at sample 245. Linear chirp sweep from 313 to 375Hz over duration of 500 samples. 64 sensors. Spacing d=1.88m. Processing band 280-400Hz. Sampling rate 1kHz. Snapshot length 128 time samples. 12 beams.

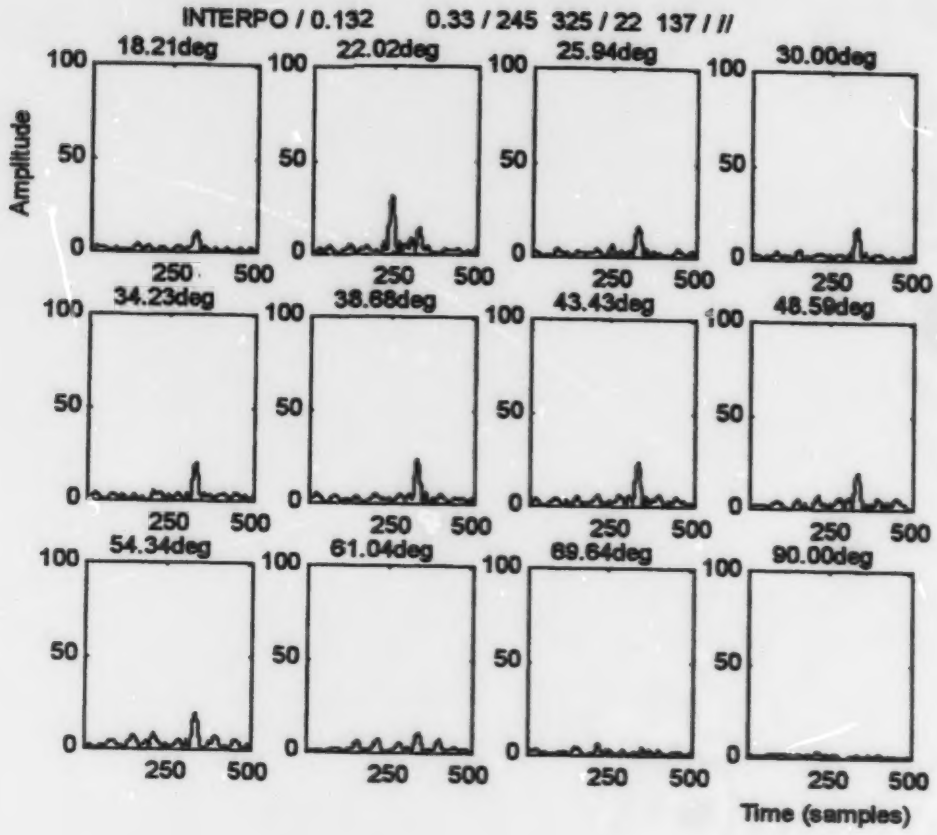

Fig. 4.4. Correlator output for WB Interpolation beamformer. Bent line array. Bow = 10m. Shows effect of signal in vicinity of conjugate bearing.

Two chirp sources: Stronger at 137^0, arrival time at sample 325; weaker at 22^0, arrival time at sample 245. Linear chirp sweep from 313 to 375Hz over duration of 500 samples. 64 sensors. Spacing d=1.88m. Processing band 280-400Hz. Sampling rate 1kHz. Snapshot length 128 time samples. 12 beams.

5. Conclusion

The interpolation beamformer has been demonstrated to offer a computationally efficient approach to narrowband beamforming with a bent array. A simple rule-of-thumb has been introduced which, for Kaiser-Bessel shading, enables the requisite number of interpolation coefficients to be predicted for any given narrowband, planewave scenario involving a uniform line-array bent into an arc of a circle of known radius.

The beamformer has been shown to be competitive in performance with the conventional, but generally less efficient, delay-and-sum beamformer, with a beam response generally within 0.1dB of the delay-and-sum benchmark over the important mainlobe and near-in sidelobes. The interpolation beamformer's output has to be considered for bearings over the complete 360^0 range and there is a negative feature in that its beampattern may have a rather broad lobe in the general vicinity of the conjugate beam angle i.e. at bearings in the neighbourhood of (180^0 - steering direction). However, this broad lobe, whose width is a function of array curvature, is also present in the benchmark delay-and-sum beamformer and is thus not a problem unique to the interpolation beamformer, itself. Indeed the interpolation beamformer may be viewed as a derivative of the delay-and-sum method.

Finally, it has been demonstrated via numerical simulations, that the interpolation beamformer may be successfully employed in a wide-band, active sonar scenario involving linear FM chirp signals and correlation detection.

6. References

[1-1] D.B. Dalrymple, "Mapping a 200 element, 300 beam curvature correcting line array beamformer into COTS octal TMS320C40 VME boards," in Proc. Int. Conf. on Signal Processing Applications and Technology (ICSPAT '97), held 14-17 Sept. 1997 in San Diego, CA, pp. 793-797.

[2-1] G.L. DeMuth, "Frequency domain beamforming techniques," in Proc. IEEE Int. Conf. on Acoustics, Speech, and Signal Processing (ICASSP '77), held 9-11 May 1977 in Hartford, CT, pp. 713-715

[4-1] D. N. Swingler, D. N., "Steered adaptive subarray beamforming," DREA Contractor Report, 1998.

UNCLASSIFIED
SECURITY CLASSIFICATION OF FORM
(highest classification of Title, Abstract, Keywords)

DOCUMENT CONTROL DATA

(Security classification of title, body of abstract and indexing annotation must be entered when the overall document is classified)

1. ORIGINATOR (the name and address of the organization preparing the document.. Organizations for whom the document was prepared, e.g. Establishment sponsoring a contractor's report, or tasking agency, are entered in section 8.)

Saint Mary's University
Halifax, Nova Scotia
Canada B3H 3C3

2. SECURITY CLASSIFICATION (overall security classification of the document including special warning terms if applicable).

UNCLASSIFIED

3. TITLE (the complete document title as indicated on the title page. Its classification should be indicated by the appropriate abbreviation (S,C,R or U) in parentheses after the title).

Interpolation Beamforming for a Bent Array

4. AUTHORS (Last name, first name, middle initial. If military, show rank, e.g. Doe, Maj. John E.)

David N. Swingler

5. DATE OF PUBLICATION (month and year of publication of document)	6a. NO .OF PAGES (total containing information Include Annexes, Appendices, etc).	6b. NO. OF REFS (total cited in document)
September 1999	58	3

7. DESCRIPTIVE NOTES (the category of the document, e.g. technical report, technical note or memorandum. If appropriate, enter the type of report, e.g. interim, progress, summary, annual or final. Give the inclusive dates when a specific reporting period is covered).

CONTRACTOR REPORT

8. SPONSORING ACTIVITY (the name of the department project office or laboratory sponsoring the research and development. Include address).

Defence Research Establishment Atlantic
PO Box 1012, Dartmouth, NS, Canada B2Y 3Z7

9a. PROJECT OR GRANT NO. (if appropriate, the applicable research and development project or grant number under which the document was written. Please specify whether project or grant).	9b. CONTRACT NO. (if appropriate, the applicable number under which the document was written).
Project 1cc11	W7707-8-5996
10a ORIGINATOR'S DOCUMENT NUMBER (the official document number by which the document is identified by the originating activity. This number must be unique to this document.)	10b OTHER DOCUMENT NOs. (Any other numbers which may be assigned this document either by the originator or by the sponsor.)
	DREA CR 1999-072

11. DOCUMENT AVAILABILITY (any limitations on further dissemination of the document, other than those imposed by security classification)

(X) Unlimited distribution
( ) Defence departments and defence contractors; further distribution only as approved
( ) Defence departments and Canadian defence contractors; further distribution only as approved
( ) Government departments and agencies; further distribution only as approved
( ) Defence departments; further distribution only as approved
( ) Other (please specify):

12. DOCUMENT ANNOUNCEMENT (any limitation to the bibliographic announcement of this document. This will normally correspond to the Document Availability (11). However, where further distribution (beyond the audience specified in (11) is possible, a wider announcement audience may be selected).

Unlimited

UNCLASSIFIED
SECURITY CLASSIFICATION OF FORM

13. ABSTRACT (a brief and factual summary of the document. It may also appear elsewhere in the body of the document itself. It is highly desirable that the abstract of classified documents be unclassified. Each paragraph of the abstract shall begin with an indication of the security classification of the information in the paragraph (unless the document itself is unclassified) represented as (S), (C), (R), or (U). It is not necessary to include here abstracts in both official languages unless the text is bilingual).

The performance of a computationally-efficient interpolation beamformer is investigated. For each snapshot, each beam's output is formed from the weighted sum of relatively few Fourier coefficients taken from the Fast-Fourier transform of the narrowband sensor data. The weights perform an interpolation action on the Fourier coefficients and can be chosen to offer both array shading and bend compensation. A simple rule-of-thumb is given for the minimum number of weights necessary for Kaiser-Bessel shading of a uniform line-array bent into an arc of a circle of known radius.

It is demonstrated, via numerical simulations, that such an interpolation beamformer has a beampattern which is within about 0.1 dB of that of the benchmark delay-and-sum beamformer over the important mainlobe and near-in sidelobes.

It is also shown that the interpolation beamformer can be used in a wideband active sonar scenario involving linear FM chirps and correlation detection.

14. KEYWORDS, DESCRIPTORS or IDENTIFIERS (technically meaningful terms or short phrases that characterize a document and could be helpful in cataloguing the document. They should be selected so that no security classification is required. Identifiers, such as equipment model designation, trade name, military project code name, geographic location may also be included. If possible keywords should be selected from a published thesaurus. e.g. Thesaurus of Engineering and Scientific Terms (TEST) and that thesaurus-identified. If it not possible to select indexing terms which are Unclassified, the classification of each should be indicated as with the title).

Array
Beamforming
Curvature
Interpolation
Sonar